The Engineering and Control of Cell-toxic Nanoparticles

Radhika Mehta

A Thesis Submitted for the Degree of

Master of Science by Research

Michaelmas 2011

Inorganic Chemistry

St. Peter's College

University of Oxford

ACKNOWLEDGEMENTS

I wish to thank all the people who supported me throughout the course of this project.

Firstly, my supervisor, Dr. Jason Davis for giving me the opportunity to carry out research in his group in this interesting and multi-disciplinary area. The research in this field carried out by me and many other researchers in the past has opened my eyes to the vast and varied field of nanotechnology and nanomedicine. His constant support, guidance and valuable inputs throughout the course of my tenure are greatly appreciated.

Next, I would like to thank my college advisor, Prof. Mark Moloney who supported me in both my academic and personal endeavours at Oxford.

I would also like to acknowledge the support and cooperation of our collaborator- Prof. Ian Thompson and Andrea Chan during the course of this project.

A big thank you to my colleague, Wen-Yen Huang for teaching, guiding and helping me throughout this work. Special thanks also to Gemma-Louise Davies for her continued encouragement and valuable inputs.

I am grateful to all the departmental staff in PTCL, ICL and CRL who continued to help me with the use of equipments and facilities. Special thanks to Dr. Robert Jacobs for his continued patience and guidance with the surface analysis facilities. Special thanks also to Dr. Michael Hayward and Fabio Denis for the use and training on thermogravimetric facilities.

I am thankful to Dr. Kerstin Jurkschat for her help and training with the facilities at Begbroke Science Park, Oxford. I would also like to acknowledge Andrew Allen for access and training on TEM facilities at Harwell Research Complex, Oxford.

Special thanks to all the college staff for their support with administrative, technical and personal work.

I would also like to thank all the past and present Davis group members for their continued support and inputs both within and outside the laboratory. To Giulia, Habib, Amol, Mike and Josh for their constant cooperation, guidance and companionship. I wish them all the very best for their future.

Lastly, a big thank you to my entire family and friend circle for being with me throughout my journey here, even virtually so. This tenure has definitely being a wonderful learning experience- and has helped me evolve academically as a researcher.

The Engineering and Control of Cell-toxic Nanoparticles

Radhika Mehta
St. Peter's College, University of Oxford
Master of Science by Research in Inorganic Chemistry
Michaelmas Term 2011

ABSTRACT

In this project, native and functionalised mesoporous silica nanoparticles (MSNs) are synthesised and explored for their use as antibacterial delivery vehicles. These antibacterial loaded MSNs contribute significantly to the developing field of nanomedicine. This work broadly entails nanoparticle generation, characterisation, functionalisation, nanoparticle-bacteria cell viability studies and cell confocal imaging.

Silica nanoparticles possess tunable surface chemistry, are thermally stable up to 800°C and are suitable for cell-study due to their low toxicity at sub-100 μg/ml concentrations. The preparation of silica nanoparticles with mesopores offers great potential for their use in a variety of applications; by loading or doping them with drugs, dyes, and imaging agents. In the present study, mesoporous silica nanoparticles with amino, carboxyl, PEG and lactose functionalities are prepared and characterised to determine their size, surface charge, surface area and purity using techniques including transmission electron microscope, dynamic light scattering, zeta potential, nitrogen adsorption-desorption and thermo gravimetric analysis. These particles are subsequently loaded with hydrophobic and volatile antibacterial oils- allyl isothiocyanate and cinnamaldehyde to determine the delivery dosage, release kinetics and need for capping. The silica surface is functionalised with lactose as a capping agent due to its inherent biocompatibility and potential for bio-triggering of hydrolysis in bacterial cells such as *Escherichia coli*. It is hoped that lactose

acts as a suitable stopper *via* cross-linking the surface with intramolecular hydrogen bonding. Cell viability assays are carried out with antibacterial loaded MSNs to demonstrate bacterial cell killing and its killing efficiency. Thus the mesoporous nanoparticles are envisaged as efficient and colloidally stable antibacterial delivery systems.

ABBREVIATIONS

AITC	Allyl isothiocyanate
APTES	3-aminopropyltriethoxysilane
ATP	Adenosine triphosphate
° C	degrees Celcius
cm^{-1}	wavenumbers
CTAB	Cetyltrimethyl ammonium bromide
DI water	De-ionised water
DLS	Dynamic Light Scattering
DMEM	Dulbecco's Modified Eagle Medium
DMF	dimethylformamide
DMSO	dimethyl sulphoxide
DOTA	1,4,7,10-tetraazacyclododecane-1,4,7,10-tetraacetic acid
DOX	Doxorubicin hydrochloride
E.coli	*Escherichia coli*
EPS	Extracellular polymeric substance
f-MSN	fluorescent MSN
FTIR	Fourier Transform Infrared Spectroscopy
g	grams
Gd	gadolinium
HCl	hydrochloric acid
MIC	Minimum Inhibitory Concentration
mg	milligram
Mg	Magnesium
$MgCl_2$	Magnesium chloride
mL	millilitres
mmol	millimoles
mM `	millimolar
MRI	Magnetic Resonance Imaging
MSN	Mesoporous silica nanoparticle

mV	milliVolts
NH_4OH	ammonium hydroxide solution
nm	nanometres
OD600	Optical density at 600 nm
ONPG	ortho-nitrophenylgalactoside
PBS	Phosphate Buffer Saline
PDI	Polydispersity Index
PEG	polyethylene glycol
PI	propium iodid
PPTS	pyridinium p-toluene sulphonate
ROX	5(6)-carboxy-X-rhodamine-N-succinimidylester
RTIL	Room-temperature Ionic Liquid
SEM	Scanning Electron Microscopy
SiO_2	silicon dioxide (silica)
TEA	triethanolamine
TEM	Transmission Electron Microscopy
TEOS	tetraethyl orthosilicate
TGA	Thermogravimetric analysis
UV	Ultraviolet
λ_{em}	wavelength of emission
λ_{ex}	wavelength of excitation

TABLE OF CONTENTS

		Page No.
Chapter 1	**Introduction**	**1**
1.1	Silica Nanoparticles	2
1.2	Mesoporous Derivatives	3
1.3	MSN Delivery Systems	5
1.4	Antibacterial Nanoparticles	6
1.5	Naturally Occurring Antibacterial Oils	7
1.6	Capping Agent for Oils	9
1.7	Lactose Capping Reaction	10
1.8	Lactose Utilisation in *Escherichia coli*	11
1.9	Beta-galactosidase	12
Objectives		14
Chapter 2	**Experimental Secction**	**15**
2.1	Nonporous Silica Nanoparticles	15
2.2	Mesoporous Silica Nanoparticles	15
2.3	Amine-modified MSNs	16
2.3.1	Co-condensation	16
2.3.2	Grafting	17
2.4	Carboxylated MSNs	17
2.5	Fluorescent MSNs	17
2.6	Pegylation of MSNs	18
2.7	Lactose MSNs	18
2.7.1	Coupling reaction in absence of a catalyst	19
2.7.2	Postgrafting the APTES-lactose group onto MSNs	19
2.7.3	Coupling reaction in presence of a catalyst	19
2.8	Oil loading and Capping of MSNs	19
2.9	Lactose Capping of Gadolinium (Gd) doped MSNs	20
2.10	Dynamic Light Scattering and Zeta Potential	21
2.11	Transmission Electron Microscopy (TEM)	22

2.12 Thermo gravimetric Analysis (TGA) 23
2.13 Nitrogen Adsorption-Desorption 24
2.14 UV-Visible Spectroscopy 25
2.15 Fourier Transform Infrared Spectroscopy 26
2.16 Confocal Laser Scanning Microscopy 27
2.17 HeLa Cell Culture and Nanoparticle-Incubation 29
2.18 *Ecoli* Cell Studies 29
2.19 Commercial Beta-galactosidase Enzymatic Assay 30
2.20 Bacterial Biofilm Studies 32

Chapter 3 Nanoparticle Generation and Characterisation 33
3.1 Introduction 33
3.2 Aims 34
3.3 Characterisation of Prepared Nanoparticles 35
3.3.1 Solubility, Size, Surface Charge and Morphology 35
3.3.2 Porosity and Surface Area 42
3.3.3 Thermal Degradation Studies 44
3.3.4 Presence of Functionalities *via* Infrared Studies 47
3.4 Hela Cell-Nanoparticle Incubation Studies 49
3.5 Conclusions 51

Chapter 4 MSNs as Antibacterial Agents 52
4.1 Introduction 52
4.2 Aims 52
4.3 Oil Toxicity Studies 54
4.4 Nanoparticle Toxicity Studies 55
4.5 Uncapped Oil-loaded Nanoparticle Release 56
4.5.1 Allyl isothiocyanate (AITC) and Cinnamaldehyde 56
4.5.2 Rhodamine 6G 57
4.6 Lactose Coating of MSNs 59
4.6.1 Release from Oil-loaded Lactose MSNs 60

4.6.2 Water Access to Mesopores in Gadolinium doped MSNs 61
4.7 Enzymatic Removal of Lactose Cap 63
4.8 Bacterial Incubation to Study Antibacterial Activity of Loaded Nanoparticles 64
4.9 Bacterial Biofilm Confocal Study 66
4.10 Conclusions 69

Chapter 5 Conclusions and Future Work **71**

Appendices **75**

References **77**

1. INTRODUCTION

Nanoscale structures and materials have been the focus of attention for many years, due to their wide range of perceived applications in many interdisciplinary domains including chemistry, physics, materials science, engineering, biology and medicine. The term 'nanomaterial' refers to any material which has at least one dimension less than 100 nanometres in size; a nanometre is one billion times smaller than a metre. Nanoscale materials can have controllable sizes which make them potentially useful for biological applications in particular, where nanomaterials can approach an object or site of interest and can be tailored to carry out specific tasks.

The properties and functions of nanostructures often differ drastically from their bulk counterparts. This can be due to their high surface area-to-volume ratio, surface tailorability, multifunctionality and improved solubility, all of which open a multitude of new possibilities for a wide variety of applications in different fields of science and technology [1].

Nanoparticle systems are being actively studied for their applications as drug delivery agents [2-20].

The presence of mesopores increases the surface area available and offers excellent opportunities for loading them with drugs and dyes. Since silica nanoparticles are colloidally stable in many organic and aqueous solvents, they can act as carriers for both hydrophobic and hydrophilic agents. The colloidal stability and homogeneity of the mesoporous silica nanoparticles facilitate their use in biological systems. Thus the size, structure and uniformity of these particles are important factors to consider prior to their applications in drug delivery and diagnostics.

1.1. Silica Nanoparticles:

Silica nanoparticles are spherical monodisperse units of silicon dioxide (SiO_2) in the nanometre range, usually between 5 nm-200 nm in diameter depending on the method of synthesis and desired application[21-25]. They were first prepared in 1968 by Stöber *et.al* [26]. The preparation route involves acidic or basic hydrolysis of tetraesters of silicic acid (tetraalkylsilicates) followed by condensation to form silica sol-gel. The Stöber method of preparing discrete nanoparticles involves basic hydrolysis of tetraethylorthosilicate in ethanolic solutions with ammonium hydroxide. Condensation of the orthosilicic acid results in formation of a nano-silica sol (Figure 1.1).

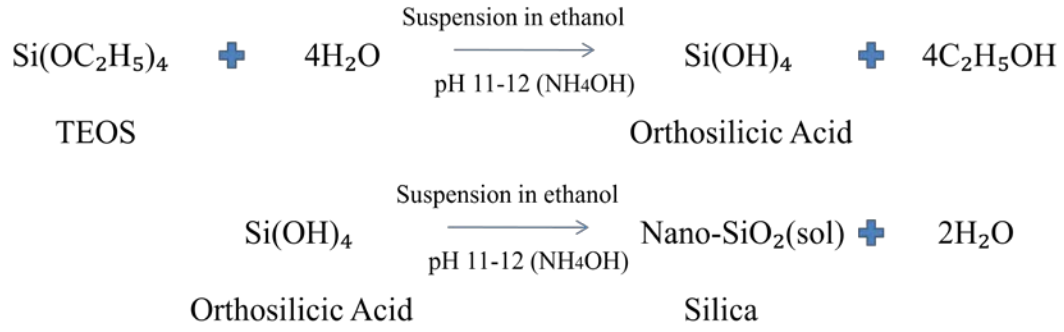

Figure 1.1: Hydrolysis and condensation of tetraethylorthosilicate (TEOS) by the Stöber method to form silica nanoparticles.

The usefulness of silica nanoparticles for medical applications lies in their chemical stability, their surface, which allows ready functionalisation and their low cytotoxicity [27-31]. Their cytotoxic effects have been studied with different cell lines and have been found to be non-toxic up to concentrations of 0.1 mg/ml [26, 32].

Mesoporous silica derivatives hold great advantages over traditional non-porous silica nanoparticles for applications in drug delivery. In addition to the inert nature of silica, the

high surface area and volume in mesoporous derivatives gives them excellent potential as multi-modal vehicles.

1.2. Mesoporous Derivatives:

Mesoporous silica nanoparticles (MSNs) are monodisperse and colloidally stable silica particles which have uniform pore size, comprised of a honeycomb-like porous structure with 'empty' channels which can encapsulate or adsorb materials. Recently, the study of MSNs has gained momentum since they open up avenues in therapeutics [5, 6, 8, 12, 14, 16, 33-36], diagnostics [7, 9-11, 37, 38] and catalysis [13, 39-41]. Their particle size, shape and porosity can be controlled during the synthetic procedure which can be suitably applied in different systems.

MSNs can be prepared by a variety of techniques, from classical aqueous and emulsion techniques to spray drying[42-44]. The most popular route for preparing MSNs is by an aqueous templating method, which utilises the Stöber hydrolysis and condensation mechanism (described in Figure 1.1). The synthetic procedure for MSN preparation involves the use of a template such as a surfactant around which silica condenses. The template is then removed to yield the mesoporous structure. The choice of template can affect the pore size of the MSNs [45, 46]. Cetyltrimethylammonium bromide (CTAB) is the most commonly used template for silica condensation. The experimental synthesis of MSNs conducted in this work involves the use of tetraethylorthosilicate (TEOS) as the silica precursor which hydrolyses in the presence of a base, triethanolamine (TEA) and condenses on CTAB in water-ethanolic suspension. TEA facilitates the reaction at a lower pH of 9 [47]. Template removal is carried out *via* acidic

hydrolysis in ethanolic hydrochloric acid (HCl)[47-49] or calcination (at 500°C) [28, 44, 50] to yield mesoporous silica nanoparticles. However, use of calcination is avoided in preparation of MSNs with organic functionalities, to avoid removal of functionalities themselves.

The particles prepared have been seen to range from 50-200 nm depending on the synthetic technique adopted [14, 47, 50-53]. During the preparation of mesoporous silica nanoparticles by the aqueous sol-gel method, careful control of the reactant ratios and the temperature at which the reaction is carried out yields nanoparticles of sizes between 50-80 nm which are ideal for biological applications. The porosity of the mesoporous particles can be tuned to range from 2-10 nm to facilitate numerous uses including adsorption of a variety chemicals and biomolecules [45, 46, 54].

The chemical and thermal stability of silica, along with its biocompatibility, makes it an ideal platform for theranostics. The surface chemistry can be tuned by reacting with different functionalities that provides scope for controlled and targeted delivery of an encapsulated substance. They are potential carriers for both hydrophobic and hydrophilic molecules with differing shapes and functionalities due to the ability to tune the porosity [8, 12, 34, 55]. It is however, observed that after drying, MSNs are occasionally difficult to redisperse. This is attributed to the formation of siloxane bridges between the surface silanol groups causing aggregation. The presence of organic functionalities on the surface of the particles may decrease the probability of formation of these bridges[14, 56, 57].

Functionalisation of the silica surface [48, 49] can be carried out *via* two methods: *in situ* co-condensation and post-synthesis grafting. The co-condensation process involves functionalisation during the synthesis of the particles and leads to high surface functionalisation [48, 50, 57, 58]. Post-grafting, which involves modification of the silanol surface after particle formation, leads to both inner mesopore and surface functionalisation. Functionalisation with groups that modify their surface charge (zeta potential) affect particles' internalisation and uptake mechanism in cellular systems [15].

The cytotoxicity of MSNs has also been widely investigated and similar results to that of the effect of amorphous silica nanoparticles in cells have been reported. That is, the viability and proliferation of mammalian cells is not affected by the internalisation of silica nanostructures into cells up to concentrations of 0.1 mg/ml [27]. An important note regarding the uptake of MSNs into cells is the effect of surface charge (*i.e.* zeta potential); MSNs with high surface charges can easily escape endosomal entrapment, an occurrence which can be attributed to osmotic pressure caused by high density of ions surrounding the surface of the highly charged MSNs [16].

1.3.MSN Delivery Systems:

MSNs are well-known as delivery agents for organics, dyes, biomolecules and adsorption of gases as stated previously[2, 6, 8, 15, 54, 59, 60]. Thanks to their good chemical stability, high surface areas, well-defined pore structures and tuneable pore sizes, they can be optimised for the doping agent of interest. Doping can be achieved by adsorption to pore walls or chemically reacting with functionalities on the silica surface. The solubility of MSNs in a variety of

organic and aqueous solvents provides for optimal choice for doping purposes. Thus both hydrophobic and hydrophilic drugs can be conveniently loaded in the mesopores of the silica nanoparticles. Many drugs and dyes have been previously loaded into the mesopore, some of which are tabulated in table 1.1.

Table 1.1: Some examples of drugs and loaded into MSNs

Doping agent	Uptake	Release
Tris(bipyridine)ruthenium(II) dichloride	0.07mg/mg MSN	0.056mg/mg MSN (80% - 24 hours) [2]
Vancomycin	0.04mg/mg MSN	0.034mg/mg MSN (85% - 72 hours)[8]
Adenosine triphosphate(ATP)	0.0024mg/mg MSN	0.002mg/mg MSN (85% - 72 hours)[8]
Doxorubicin hydrochloride (DOX)	0.265mg/mg MSN	release not quantified [2]

In recent years, considerable research has been published reporting MSN delivery systems capped with functionalities that respond to external stimuli such as light [61-65], enzymes[2, 60, 66-68], chemicals[8, 15] and pH[5, 33, 45, 46, 69, 70]. However, most of these systems are mechanised with functionalities that may be cytotoxic to different cellular systems. Hence, a simple biocompatible and bio-triggered system is designed that involves sugars as capping agents which can be readily degraded by bacterial cells. Prior work dealing with saccharides as biogates has been carried out with hydrolysed starch derivatives including glucidex 47, 39, 20 [2] and cyclodextrins [60, 61, 69, 71].

1.4. Antibacterial Nanoparticles:

Much work has been documented on the study of antibacterial nanoparticles with inherent antibacterial activity (silver nanoparticles) [72-75]. Silver nanoparticles are known to show strong

biocidal effects on bacterial cells [72, 76]. Sondi *et.al* [72], for example report a 70% inhibition of *E.coli* bacterial growth with 10 μg/ml of silver nanoparticles (size: 12.3±4.2 nm) and a 100% inhibition using 50-60 μg/ml concentrations.

Some studies report use of silica nanoparticles as delivery platforms for antibacterial agents including room-temperature ionic liquids (RTIL)[8, 77], vancomycin[8] and nitric oxide[78]. Work published by Trewyn *et.al.* [77] discusses the use of RTIL templates such as 1-hexadecyl-3-methylimidazolium bromide (C_{16}MIMBr) for synthesis of mesoporous silica materials. The controlled release of these RTIL templates from mesoporous silica materials (particle size of 100-300nm with pore volume of 0.95cm^3/g) were studied against *E.coli* cells to test their antibacterial activity. The work concluded that the antibacterial activity depended on the rate of diffusional release of the encapsulated RTILs and was affected by the particle and pore morphology of the MSNs. The minimum inhibitory concentration (MIC) – lowest concentration of a substance that inhibits visible growth for C_{16}MIMBr was determined to be 30 μM [77].

1.5. Naturally Occurring Antibacterial Oils:

In collaborative work with a team in the Department of Engineering Science, certain naturally occurring oils such as allyl isothiocyanate, cinnamaldehyde, thymol and carvacrol, have been shown to possess potent antibacterial properties. These oils (also called essential oils since they carry the distinctive scent or essence of the plant) cause inactivation of proton motive force across cell membrane, interfere with salt concentrations and other vital elements and metabolites from within the cells, ultimately leading to cell death [79-84].

Essential oils are harvested from plant material (flowers, buds, seeds, leaves, twigs, bark, herbs, wood, fruits and roots). They can be obtained by expression, fermentation, or extraction but the method of steam distillation is most commonly used for their commercial production.

The antibacterial dosage for each of the oil varies with bacterial species under investigation. In this work, studies have been carried out with allyl isothiocyanate and cinnamaldehyde (Figure 1.2).

Allyl isothiocyanate (AITC) is a major constituent of Mustard Oil (99%). It has a molecular formula C_4H_5NS, molar mass of 99.15 g/mol and UV absorbance at 245 nm [85].

Cinnamaldehyde is a major constituent of Cinnamon Oil (52-70%). It has the molecular formula C_9H_8O, molar mass of 132.16 g/mol UV absorbance at 291 nm[86].

Figure 1.2: Structural formula for allylisothiocyanate (left) and cinnamaldehyde (right).

Many studies indicate that the antimicrobial effect of essential oil constituents depend on their hydrophobicity and consequently on their partition in the cytoplasmic membrane [79, 82]. The relationship between the strength of antimicrobial and its chemical structure is important for a better interpretation of the effectiveness of the antimicrobial compounds[79]. The potential antimicrobial activity of cinnamaldehyde is attributed to the functional aldehydic group that would facilitate the interaction with molecules such as proteins and nucleic acids [87]. AITC has an amphiphilic structure and exerts its antimicrobial activity by acting on cell membrane [84]. Moreover, it could alter the protein structure by reacting with free amino groups and disulphide bonds of proteins.

The MIC for AITC and cinnamaldehyde is reported as 0.31 mM and 2.5-3 mM respectively with *E.coli* and *Salmonella typhimurium* bacterial species[80, 83]. The MIC for *Staphylococcus aureus* is reported as 0.15 mM and 2.5 mM for AITC and cinnamaldehyde respectively [80, 83]. The method for calculating these MIC values varies significantly in literature. The above data was gathered by employing 25% (v/v) ethanol as the solvent for the natural antibacterials [80]. The studies in this work are carried out in the absence of ethanol, as alcohols can contribute to antibacterial properties.

These oils are also being employed as antibacterial agents against bacterial biofilms which are aggregates of bacteria in which cells adhere to each other and/or to a surface. These are embedded within a self-produced matrix of extracellular polymeric substance (EPS) which is a polymeric conglomeration generally composed of extracellular DNA, proteins and polysaccharides. However, for preliminary work with nanoparticles, *E.coli* bacterial cells are used for the study.

1.6. Capping Agent for Oils:

AITC and cinnamaldehyde are hydrophobic and volatile in nature; this limits their miscibility, efficiency and availability to bacterial cells for *in vitro* studies. Hence, these have to be administered *via* a system that can increase delivery in aqueous solutions without loss due to volatility. Mesoporous nanoparticles present a very powerful means of delivering molecules which have inherently low aqueous solubility. In order to achieve selective delivery with particles which are, otherwise, unvectored, the concept of specific pore capping is particularly useful.

This project involves targeting to *E. coli* bacteria, hence decapping *via* enzymatic activity is preferred. *E.coli* bacterial cells produce the enzyme beta-galactosidase intracellularly that ferments lactose. Lactose, being a disaccharide, is expected to be large enough to cap the openings on MSNs by intermolecular hydrogen bondings thereby retaining the oils within the pores. Its subsequent degradation to release the antibacterial oil intracellularly would enhance its efficiency further. Thus lactose has been chosen as the capping agent for this work.

1.7. Lactose Capping Reaction:

Lactose can be coupled onto the MSN surface by reacting it with an amine group via a nucleophilic substitution reaction. In the literature, the lactose-amine reactions are known to be carried out at room temperature using an equimolar mixture of lactose and amine in ethanol-water mixture [88-90]. In the MSN system, 3-aminopropyltriethoxysilane (APTES) is used to aminate the MSN surface prior to the attachment of lactose.

The mechanism of the proposed reaction is shown in Figure 1.3.

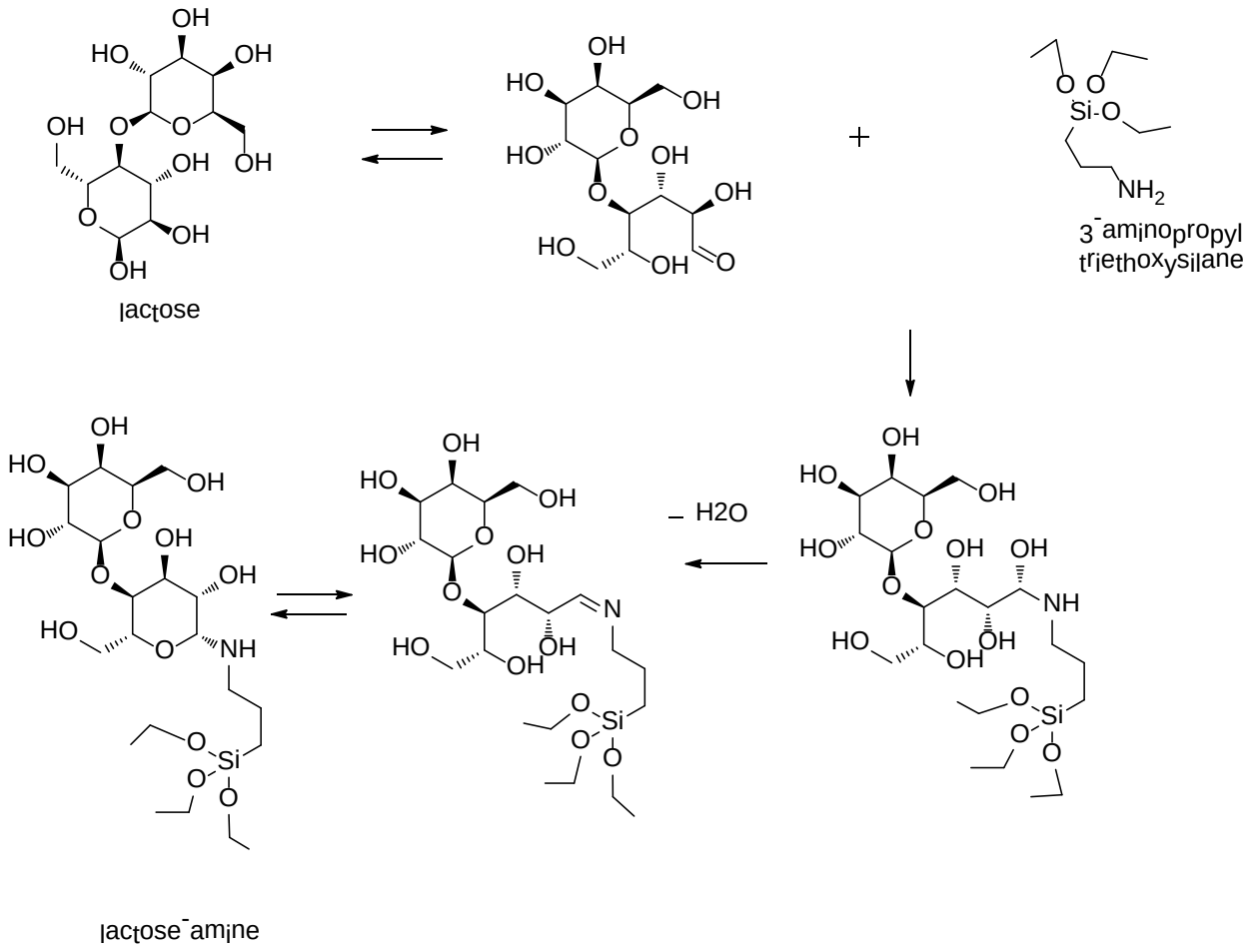

Figure 1.3: Lactose-amine coupling reaction:
The reaction mechanism involves nucleophilic substitution of the C_4-hydroxyl group with the amine group. This takes place *via* the attack of the lone pair of electrons on nitrogen onto the carboxylic carbon on the glucose moiety of lactose. It then undergoes rearrangement with the loss of a molecule of water to give the lactose-amine.

1.8. Lactose Utilisation in Escherichia coli:

The enzymatic hydrolysis of lactose by *E.coli* cells is facilitated by the lac operon (Figure 1.4) [91]. This system regulates the activities of two enzymes – lac permease and beta-galactosidase. Lac permease is a membrane bound transport protein responsible for transporting the lactose into the cell. Beta-galactosidase is the enzyme which hydrolyses lactose to galactose and

glucose, thus permitting the bacterium to live on lactose. These two enzymes are encoded by the Y and Z genes in the lac system.

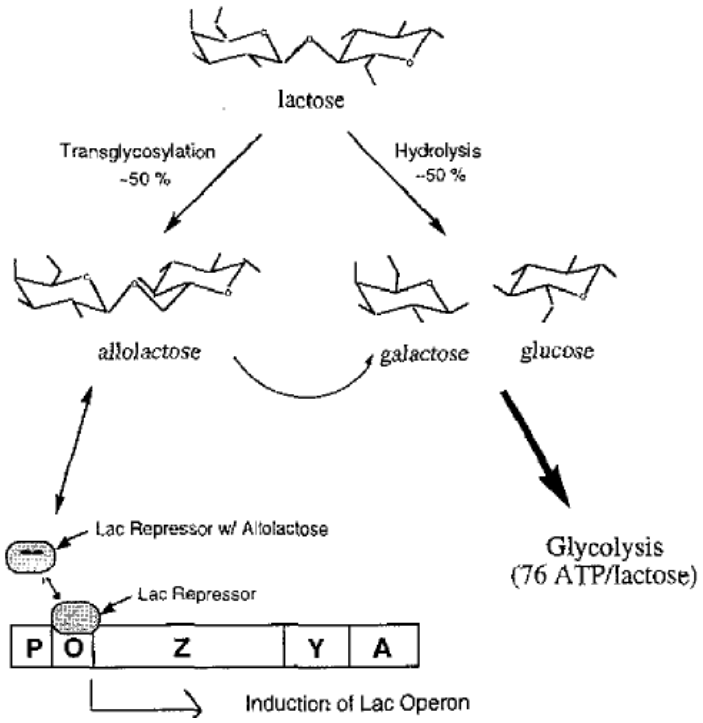

Figure 1.4: Lac operon in *E.coli* cells. Reproduced from Juers *et.al.*, Biomaterials, 2001, 40, 14781-14794.

These enzymes are expressed only when lactose is present in the bacterial environment where no other source of nutrient is present.

1.9. Beta-galactosidase:

The *in vitro* release studies from lactose capped MSNs were proposed to be carried out in the presence of the commercial enzyme beta-galactosidase. This enzyme is a hydrolase enzyme that facilitates hydrolysis of beta-galactosides into monosaccharides (galactose) and the other

organic moiety like o-nitrophenol. It has a molecular weight of about 540000 and contains a sulphydryl with 19 cysteine units and some disulphide bonds.

The optimum pH for this enzyme ranges from 6 to 8 [92]; a phosphate buffer of appropriate pH is generally used. The assay used contains Mg^{2+} salt as an activator. The optimum concentration is supposed to range from 0.1-10mM [93, 94]. Beta-mercaptoethanol acts as stabiliser for the enzyme since it can undergo oxidation due to the presence of sulfhydryl groups [95]. Also thiol reducing agent- beta-mercaptoethanol is used in presence of $MgCl_2$, since inhibition has been observed with beta-mercaprotethanol when no $MgCl_2$ is present [93, 95].

OBJECTIVES

This project explores the use of functionalised MSNs as delivery systems for naturally occurring essential oils that exhibit antibacterial properties. This work broadly entails nanoparticle generation, characterisation, functionalisation, nanoparticle- bacterial cell viability studies and cell confocal imaging.

The specific goals of the work were as follows:

1. Preparation of colloidally stable mesoporous silica particles and their full structural characterisation using DLS, TEM, zeta potential, TGA;
2. Confocal analysis of the cellular interactions of discrete, colloidally stable mesoporous silica nanoparticles with bacterial and Hela cells;
3. Investigation of the uptake and release of antibacterial oils, including AITC and cinnamaldehyde, in mesoporous silica nanoparticles and colloidal stability of the loaded particles;
4. Capping of the mesopores for controlled delivery and investigation of enzymatic decapping for oil release;
5. Examination of the antibacterial effects of the loaded mesoporous nanoparticles with bacterial cells using cell viability assays to specifically see whether nanoparticle delivery can facilitate *E.coli* cell killing at markedly lower doses than pure oil.

2. EXPERIMENTAL SECTION

Materials

All chemicals used were received from Sigma Aldrich unless otherwise stated. PEG-silane, [hydroxy(polyethylyenoxy)propyl]-triethoxysilane was obtained from Gelest. The dyes Lysotracker Green DND-26 and Hoechst 33342 for Hela cell work were obtained from Invitrogen. Bacterial cell stain, BacLight containing styo-9 and propidium iodide were also obtained from Invitrogen.

Nanoparticle Preparation

2.1. Nonporous Silica Nanoparticles[21] :

Ammonium hydroxide (NH_4OH)(1 ml) was dissolved in ethanol (EtOH) (20 ml). To this solution, tetraethylorthosilicate TEOS (1 ml, 4.48 mmol) was added drop-wise with constant magnetic stirring. The reaction was left for 24 hours. In order to separate the particles from excess reagents, the colloidal solution was centrifuged at 13200 rpm at 25° C for 15 minutes. Washing: The supernatant was then discarded and the remaining gel suspended in ethanol (2 ml) using sonication (100 Watt Power, 25-40° C). The above procedure for washing was repeated 2-3 times. The nanoparticles were retained in ethanol suspension for further characterisation. Each batch yielded 250-300 mg of nanoparticles.

2.2. Mesoporous Silica Nanoparticles:

The preparation of mesoporous silica nanoparticles(MSN) followed the protocol published by Moller *et al*.[47] This involved using cetyltriethyl ammonium bromide (CTAB) as the template

for hydrolysis and condensation of silica and the polyalcohol triethanolamine (TEA) was used as the base.

A solution of deionised water (DI water) (16.02 ml), CTAB (0.64 mg, 1.75 mmol), ethanol (1.84 g, 40.18 5mmol) and TEA (1.029 g, 6.48 mmol) was prepared and heated to 80°C prior to the addition of TEOS. TEOS (1.454 ml, 6.48 mmol) was then added drop wise and the reaction was left to stir for 2 hours at 80°C. After the reaction was complete, the particles were centrifuged down and redispersed and sonicated in acidic ethanol (100 ml ethanol, 15 ml HCl) for 30 mins twice to remove the surfactant template. The particles were then redispersed in ethanol. Each batch prepared yielded approximately 400- 450 mg of nanoparticles.

2.3. Amine Modified MSNs:

MSNs can be modified with amine in two ways- either co-condensation or post-synthesis grafting.

2.3.1. Co-condensation: The protocol followed varied depending on the concentration of amine modification. For 1:10 3-aminopropyltriethoxysilane (APTES) to TEOS ratio, initially an equimolar ratio of TEOS -APTES mixture is prepared (solution A) using TEOS (0.145 ml, 0.65 mmol) and APTES (0.132 ml, 0.65 mmol). The basic process followed is similar to unfunctionalised MSNs. A solution of deionised water (DI water) (16.02 ml), CTAB (0.64 mg, 1.75 mmol), ethanol (1.84 g, 40.185 mmol) and TEA (1.029 g, 6.48 mmol) was prepared and heated to 80°C prior to the addition of TEOS. TEOS (1.309 ml, 5.85 mmol) was added drop wise while vigorous stirring and the reaction was left to stir for an hour for initial nucleation and condensation of silica. Then solution A was added drop wise and the reaction

is stirred for another hour. Template removal was then carried out using ethanolic hydrochloric acid (HCl) as previously described.

2.3.2. Grafting: In post-synthesis grafting, unfunctionalised MSNs (after template removal) (200 mg) were dispersed in 2:1 ethanol-water mixture (30 ml total). APTES (70 μl) was added and the reaction was stirred for 24 hours at room temperature. The suspension was then centrifuged down and redispersed in ethanol. The washing procedure as stated previously was carried out in ethanol.

2.4. Carboxylated MSNs:

The preparation of carboxylated MSNs involved reacting aminated MSNs with succinic anhydride in anhydrous dimethylformamide (DMF). 10% aminated MSN (synthesised *via* post-grafting) (40 mg) was reacted with succinic anhydride (24 mg, 0.24 mmol) in anhydrous DMF (20 ml) overnight for 18 hours. Thereafter, the nanoparticles were centrifuged down and washed with ethanol as above.

2.5. Fluorescent MSNs:

Preparation of fluorescent MSNs(f-MSN), was carried out by ethyl dimethylaminopropyl carbodiimide (EDC) coupling of the fluorophore ROX 5(6)-carboxy-X-rhodamine-N-succinimidylester (2 mg, 1.58 μmol) to the amine group on the aminated MSNs. The aminated MSN was prepared *via* the co-condensation method described previously. Following template removal, ROX was stirred with aminated MSN (400 mg) in ethanol (15 ml) for 24 hours. It was then washed with ethanol via sonication and centrifugation.

The scheme for carbodiimide coupling is shown below:

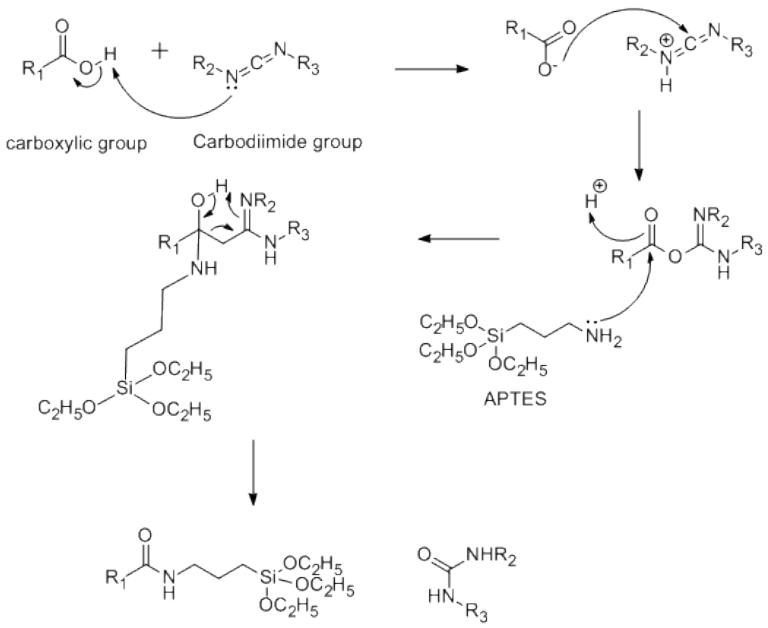

Figure 2.1: Scheme for carbodiimide coupling of 3-aminopropyltriethoxysilane (APTES) to a carboxylic acid functional group.

2.6. Pegylation of f-MSNs:

Pegylated MSNs were prepared by mixing f-MSNs with [hydroxy(polyethylyenoxy)propyl]-triethoxysilane (PEG), molecular weight 350-750 g/ml in 50% ethanol. PEG was reacted with fluorescent MSN (50 mg) in ethanol (5 ml) and water (2.5 ml) with vigorous stirring for 24 hours. The concentration of PEG was varied between 0.05-0.1 mmol (75 μl) in order to yield particles with different loadings of PEG. The washing procedure of sonication and centrifugation was followed in ethanol.

2.7. Lactose MSNs:

In order to prepare lactose functionalised particles, lactose was coupled to APTES on amine-modified MSNs. The concentration of APTES on MSNs was calculated to be 0.08 mmol APTES on 60 mg of APTES MSN, assuming complete amination. Thus, APTES MSN (about

0.08 mmol APTES, 60 mg) was dissolved in absolute ethanol (4 ml). Two methods were followed:

1.7.1. Coupling reaction in absence of a catalyst: To the reaction mixture lactose (60mg, 0.16 mmol) in DI water (2 ml) was added and kept for stirring at room temperature for 24 hours after which it was centrifuged down and washed several times with ethanol and water. Variations to this method were carried out by (a) heating the reaction at 60°C (b) changing APTES:lactose molar ratios from 1:2 to 1:1, 1:5 and 1:10 (c) reacting MSNs and lactose in phosphate buffer (6 ml, 0.1 M) pH 4 and pH 7 (d) increasing the reaction time to 48 hours. The washing in water and ethanol were carried out as discussed previously.

2.7.2. Postgrafting the APTES-lactose group onto MSNs: The lactose-APTES derivative was prepared by reacting lactose (1.875 g, 3 mmol) with APTES (0.6 ml, 3 mmol) in ethanol (50 ml) over 24 hours. Thereafter, the reaction mixture was heated to 60°C for 30 minutes and the solvent was evaporated using a rotavapour to obtain a white solid. 80 mg of this solid was added to MSN (40 mg) in DI water (10 ml) and the reaction was stirred for 5.5 hours. The washing in ethanol and water was carried out as discussed previously.

2.7.3. Coupling reaction in presence of a catalyst: To the reaction mixture lactose (60 mg, 0.16 mmol) and pyridinium p-toluene sulphonate (PPTS) (3.8 mg, 0.016 mmol) in 1.5 ml water was added and kept for stirring at room temperature for 24 hours after which it was centrifuged down and washed several times with ethanol and water.

2.8. Oil loading and Capping of MSNs:

To load the antibacterial oil in the mesopores of the nanoparticles, 8 ml of 15 mg/ml of APTES-MSN (0.16 mmol APTES) in ethanol was doped with varying concentrations of the

oils- allylisothiocyanate and cinnamaldehyde (1 µl/ml, 10 µl/ml and 50 µl/ml). For rhodamine 6G, 1 mg/ml and 10mg/ml concentrations were used. The mixture was stirred at room temperature for 48 hours to observe maximum loading. Aliquots of the mixture were centrifuged down at different intervals and the absorbance of the supernatant was studied. The uptake and release was followed spectroscopically at 245 nm for AITC (see Appendix for UV-Vis Spectra), 291 nm for cinnamaldehyde (see Appendix for UV-Vis Spectra) and 529 nm for rhodamine 6G.

For capping, the above reaction mixture was stirred for 24 hours since maximum loading was achieved by then. Thereafter, lactose (120 mg, 0.32 mmol) and PPTS (7.6 mg, 0.032 mmol) in 4 ml water was added to the loading mixture and stirred for another 24 hours at room temperature. Finally, the mixture was centrifuged down and washed several times with ethanol and water.

2.9. Lactose Capping of Gadolinium (Gd) doped MSNs:

1,4,7,10-tetraazacyclododecane-1,4,7,10-tetraacetic acid (DOTA) is used as the chelate for gadolinium doping in MSNs. The DOTA was incorporated by dispersing MSNs (300 mg) in dimethylformamide (DMF) (6 ml) and adding triethylamine (640 µl, 4.59 mmol) and DOTA-NHS-ester (10 µmol). The solution was stirred at room temperature for 24 hours. Thereafter, the DOTA-MSN were centrifuged and dispersed in ethanol (10 ml). Gadolinium chloride (5 mg, 20 µmol) was added to the solution and stirred at room temperature for 24 hours. Unwashed Gd was removed by washing the as-synthesised particles with absolute ethanol.

For capping, the MSN surface was initially post-grafted with 10% APTES. Following this, APTES –Gd-MSN (40 mg) were dispersed in 3 ml ethanol and reacted with lactose (40 mg, 0.11 mmol) in 1.5 ml DI water for 24 hours at room temperature. The particles were then centrifuged and washed as stated previously.

Analytical Instruments and Techniques

2.10. Dynamic Light Scattering and Zeta Potential:

DLS is a technique used to measure the hydrodynamic size of particles in the sub-micron range. It provides information about the average particle size in suspension and also measures the width of the particle distribution, called the polydispersity index (PDI). In DLS, colloidal samples are illuminated with a laser that leads to scattering of light. This scattering is correlated to the Brownian motion of particles which relates it to the size of the particles.

Zeta potential provides valuable information about the surface charge of sub-micrometre particles. Depending on the surface functionality, net charge can develop on the particle surface. The solvated particle then has two surrounding layers- an inner region (Stern layer) where the ions are strongly bound and an outer (diffuse) region where they are less firmly associated. Within the diffuse layer there is a notional boundary inside which the ions and particles form a stable entity. When a particle moves, ions within the boundary move along with it while those beyond the boundary stay with the bulk dispersant. The potential at this boundary is the zeta potential (Figure 2.1). The magnitude of the zeta potential gives an indication of the potential stability of the colloidal system. If all the particles in suspension have a large negative or positive zeta potential then they will tend to repel each other and there will be no tendency for the particles to come together. However, if the particles have

low zeta potential values then there will be no force to prevent the particles coming together and flocculating. The general value for highly stable suspensions is taken either higher than +30 mV for positively charged particles or -30 mV for negatively charged particles.

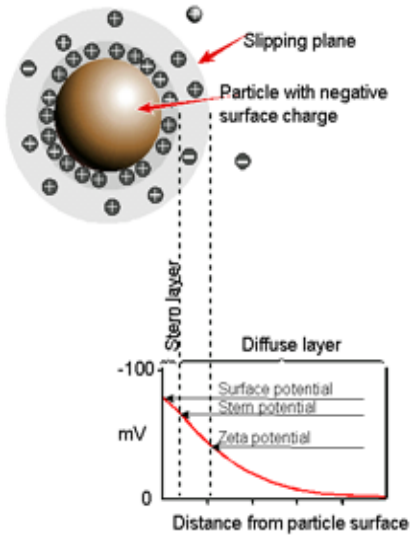

Figure 2.2: Schematic representation of zeta potential reproduced from Malvern Instruments Ltd, UK.

DLS and zeta potential measurements were taken using a Zetasizer Nano (Malvern Instruments). The zeta potential facilities were located at BegbrokeNano, Oxford. For DLS measurements, a sample solution of 10 mg/ml of particles was prepared in deionised water as solvent. These measurements were repeated in ethanol as well. For studying zeta potential, samples were prepared using concentrations of 1mg/ml in deionised water (pH 7.4).

2.11. Transmission Electron Microscopy (TEM):

TEM can provide details on the morphology of a sample[96]. In this technique, a beam of electrons are accelerated towards the sample, where lenses and apertures focus the beam precisely onto the sample. Unscattered transmitted electrons pass through the sample without

any interactions and are imaged onto a phosphor image screen or photographed with a camera.

TEM images were taken at Research Complex at Harwell, Oxford with Wen-Yen Huang and Gemma-Louise Davies. Experiments were carried out on a JEOL 2100 analytical TEM, which has a LaB_6 electron gun and can be operated between 80 and 200 kV. This instrument has a resolution of 0.19 nm. The TEM samples were prepared by dropping concentrations of 1 mg/ml of nanoparticle solution in water or ethanol onto formvar-coated copper mesh TEM grids.

2.12. Thermo gravimetric Analysis (TGA):

TGA measurements were performed to study weight loss of sample on thermal treatment- an indicator of the presence of different functionalities and the purity of the sample. The weight loss *via* TGA demonstrates the evaporation (like water) and the degradation of chemical functionalities (like hydrocarbons).

The measurement was performed on Netzsch TGA instrument in Department of Chemistry, Oxford. For the analysis, 20 mg of dry powder nanoparticle samples were taken in a ceramic crucible. The temperature was increased at a rate of 5°C/min starting at room to a maximum of 600-800°C under an inert argon atmosphere.

2.13. Nitrogen Adsorption-Desorption:

The nitrogen adsorption-desorption experiments were carried out on the Sorptomatic 1990 instrument at the Surface Analysis Facility, Department of Chemistry, Oxford to determine the porosity and surface area parameters. Physisorption of nitrogen gas on porous materials was used to determine their specific surface area and mesopore size distribution. Prior to starting the run, it was necessary to completely degas the samples in the sample holder. Thereafter, known amounts of the adsorbate (nitrogen) are introduced to the sample holder which is kept at liquid nitrogen (77 K). Adsorption of nitrogen onto the sample causes the pressure to slowly decrease until an equilibrium pressure is established in the manifold. The equilibrium pressures and the amount of gas adsorbed for each step are obtained from these measurements. The gas uptake is calculated directly from the equilibrium pressure values. A calibration with a blank run is performed before each sample. The time required to generate an isotherm ranged from 4 to 7 days depending on the porosity of the particles and the ability to completely degas the blank and samples before each run.

In this analysis, 100 mg of dried powder samples were degassed at 200°C for at least 12 hours before taking adsorption measurements.

2.14. UV-Visible Spectroscopy:

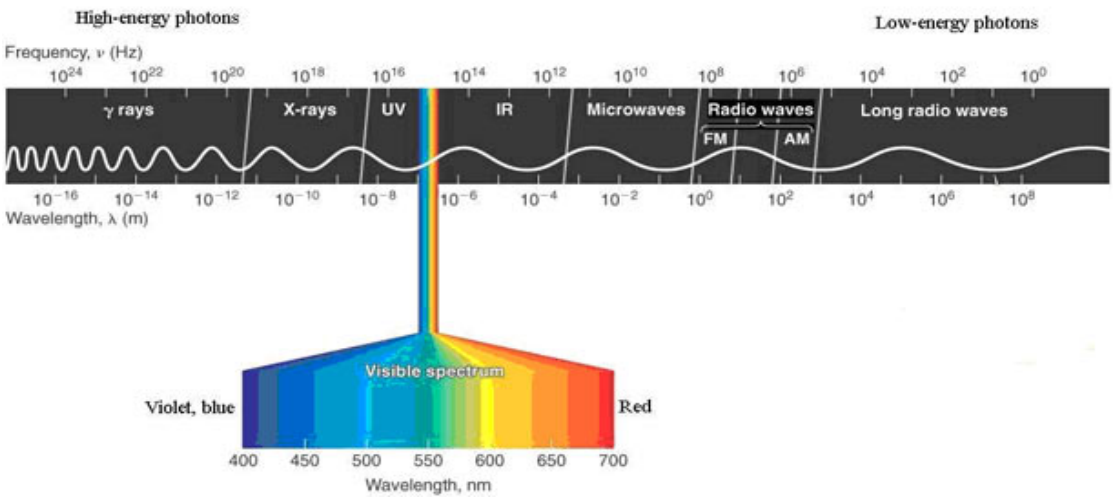

Figure 2.3: Electromagnetic spectrum showing wavelength in metres reproduced from Scientific Committee on Emerging and Newly Identified Health Risks, Light Sensitivity (2008), Scientific Rationale, p. 10.

UV-visible spectra arise due to the absorption of a beam of incident photons by a sample. The absorbance by the UV spectrometer is determined by the Beer-Lambert law, which states that the absorption of light (***A***) is directly proportional to the path length of the cell used (***l***) and the concentration (***c***) of the sample under investigation.

$$A = \varepsilon\, c\, l$$

where ε is the extinction coefficient of the substance (M^{-1} cm^{-1}).

On excitation of the valence electrons in a molecule by the incident light, electronic transitions occur from the ground state to the excited state. The frequency (and also the intensity) of the absorbed photon is directly proportional to the energy difference between these levels. The wavelength of absorption of radiation is characteristic of the material under investigation. The more easily excited the electrons (i.e. lower energy gap) the higher the wavelength of light it can absorb.

UV-visible spectroscopy was carried out on a UV PC-2401 (Shimadzu) using a quartz cuvette. The absorbance was gathered for wavelengths ranging from 200 nm to 800 nm.

2.15. Fourier Transform Infrared Spectroscopy:

Infrared spectroscopy is a technique based on the interaction of materials with radiation in the infrared region of the electromagnetic spectrum (Figure 2.2). These interactions cause excitation of the vibrational (bending and stretching modes) modes within molecules, which can be detected due to the absorption or transmittance of the infrared radiation [97]. A molecule can be considered as having bonds with spring-like properties. Movement of the bonds between atoms can include stretching (both symmetric and asymmetric) and bending vibrations [97, 98]. In the absorption process, those frequencies of IR that match the natural vibrational frequencies of the molecule in question are absorbed, and the energy absorbed serves to increase the amplitude of the vibrational motions of the bonds in the molecule. It is noted that only those bonds that have a dipole moment that changes as a function of time are capable of absorbing IR. Vibrations which show no change in the dipole moment are infrared inactive. A transmission infrared spectrum is a plot of the radiation absorbed versus the frequency of the incident radiation in wavenumbers (cm^{-1}).

The IR spectra for different samples were recorded on the FTS6000 Fourier Transform IR spectrometer built by Bio-Rad. An Attenuated Total Reflectance (ATR) accessory – DuraSamplIR diamond detector is used to study IR spectra for the nanoparticles. Here, the beam of the spectrometer is directed in to a prism at an angle which exceeds the critical angle. As the beam is directed in to the crystal at an angle which exceeds the critical angle, internal

reflections take place. When a sample is placed in optical contact with the prism at the point at which an internal reflection occurs, the sample absorbs IR energy at wavelengths equivalent to those which would be noted in a transmission experiment.

The spectra were recorded over 800-4000 cm^{-1}. The background scan was run 512 times and each sample 256 times. After installing the accessory and connecting the purge tube, there was a wait of several hours, so that all moisture is removed from the accessory. For each analysis, 10 mg of solid nanoparticle samples were placed on the diamond detector. The solid samples were mechanically pressed in to contact with the crystal to achieve optical contact.

2.16. Confocal Laser Scanning Microscopy:

This technique uses a light source that is directed through an aperture, then an objective lens. The light is thus focused to a small point on the sample, and reacted back. The beam is split, passed through another aperture, and possibly a fluorescence filter if the sample is fluorescent. It is finally collected by a photomultiplier tube and detector. Thus a point by point image is built up and put together by a computer. With a laser scanning set up, the control of the depth of focus is greater and so gives higher quality images. Fluorescent markers can be used to increase contrast and localise bodies (e.g. the DNA or the membranes).

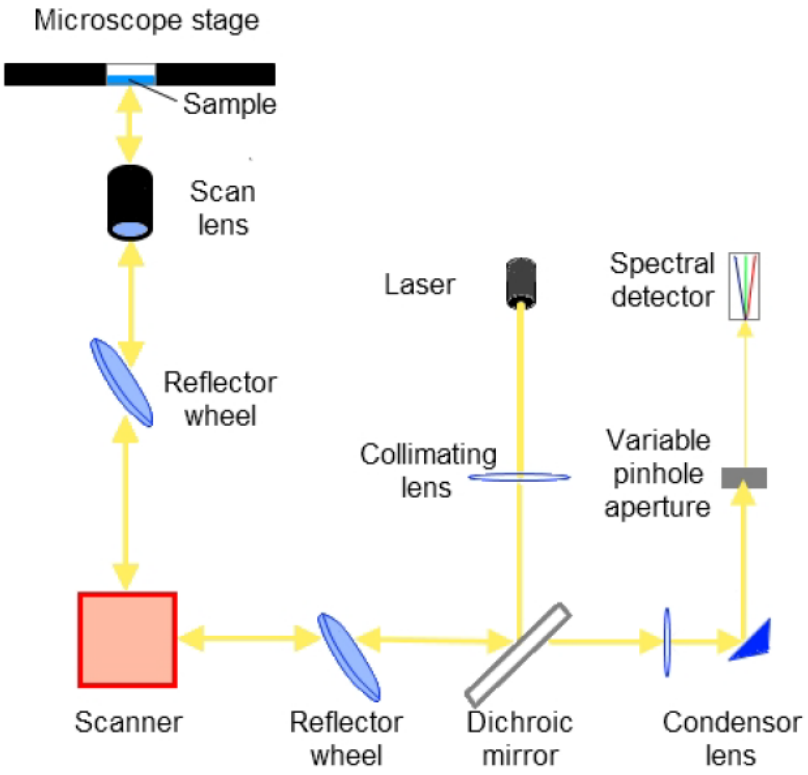

Figure 2.4: Set-up for confocal laser scanning microscopy

Confocal images were taken in the Nikon Oxford Molecular Imaging Centre (NOMIC) using a Nikon Eclipse Ti-E inverted microscope with an A1 confocal laser microscope system attachment. The microscope was fitted with a Plan Fluor 10x objective and a Plan Apo 100x oil immersion objective. The system was equipped with four laser lines (with options of 405 nm, 488 nm, 561 nm and 639 nm). NIS-Elements AR 64bit 3.00 SP6 software was used to capture and manipulate images.

The software allows the use of several techniques to obtain information. Confocal microscopy was used to study the internalization of nanoparticles within cells.

HeLa and Bacterial Cell Work

2.17. HeLa Cell Culture and Nanoparticle-Incubation:

The HeLa cells used in this project were grown using growth medium composed of Dulbecco's Modified Eagle Medium (DMEM) with Glutamax (445 ml), penicillin/streptomycin (5 ml) and fetal bovine serum (50 ml). Nanoparticles at a concentration of 0.2 mg/ml were dispersed in growth medium. HeLa cells were incubated in growth medium (2 ml) for 24 hours. The medium was removed and replaced with 1 ml of the nanoparticle suspension and 1ml of growth medium, and the cells were left to incubate for 3 hours (f-MSNs) and 30 hours (pegylated f-MSN). The medium was again removed from the suspension and the cells were washed with Phosphate Buffer Saline (PBS). The lysosomes were stained by incubation with Hoechst 33342-blue stain (1 μl/ml in PBS) for 15 minutes at room temperature. The dye solution was removed and the cells were then washed with PBS. The nucleus was stained by incubation with Lysotracker Green DND-26 (1 μl in 15 ml of PBS) for 20 minutes at room temperature. The nuclear dye solution was removed and the cells were washed again with PBS. PBS was then added to the petri dish to observe the cells under the confocal microscope.

2.18. E.coli Cell Studies:

The *E.coli* cell incubation and experimental work was carried out by Andrea Chan. The cells were grown in Minimal Davis Medium with 20% dimethyl sulphoxide (DMSO) and 0.5% Tween20 for 24 hours at 37°C (up to a density of 10^6 cells/ml) in a shaking incubator with 250 rpm, after which they were centrifuged and suspended in phosphate buffer for incubation studies.

2.18.1. Oil Toxicity Studies: The toxic dosage of the oils required for antibacterial activity was determined by the microdilution test. In this experiment, a single bacterial species was treated with oil concentrations ranging from 2500mg/L to 9.77mg/L. The cells were studied in 200 µl measuring 96- microwell plates and the optical density at 600 nm (OD600) was monitored spectroscopically for cell growth in bacterial suspensions [99].

2.18.2. E.coli cell- Nanoparticle Incubation Studies: Cell viability studies were carried out by to determine nanoparticle toxicity towards bacterial cells. Cell viability is analysed by morphological changes or by changes in membrane permeability inferred by the uptake and retention of certain dyes. Here, nonviable (dead or damaged) cells are stained by the fluorescent, DNA-binding probe propidium iodide (PI) and the fluorescence is monitored on flow cytometer (excitation at 488 nm and emission collected at >550 nm). The cells were incubated with nanoparticles at varying concentrations (1 mg/ml, 2 mg/ml or 5 mg/ml) to study the cell viability over 18 hours.

For cell viability study via flow cytometry, 1 µl of 2 mg/ml propidium iodide (2 µg/ml final) was added to approximately 10^6 washed cells (after 24 hour incubation as stated earlier) suspended in 1 ml PBS.

2.19. Commercial Beta-galactosidase Enzymatic Assay:

The commercial beta-galactosidase was used to study the enzymatic release of the loaded dye on hydrolysis of lactose. Its activity was studied using ortho-nitrophenylgalactoside (ONPG) as the substrate.

The enzyme was assayed in 3 ml reaction mixtures. Phosphate buffer of pH 7.3 (2.6 ml, 100 mM) was mixed with $MgCl_2$ in DI water (0.1 ml, 30 mM) and beta-mercaptoethanol in DI water (0.1 ml, 3.32 M).

For testing the enzyme activity ONPG solution in phosphate buffer (0.1 ml, 68 mM) were added to the above solution followed by the addition of the enzyme (0.1 ml, 0.2-1 unit/ml). A blank solution was tested where instead of enzyme solution; 1ml phosphate buffer is used. The temperature was maintained at 37^0C and absorbance at 410 nm is noted against the blank. The final concentration of each component in the reaction mixture was: 93 mM sodium phosphate, 2.3 mM ONPG, 1 mM $MgCl_2$, 112 mM beta-mercaptoethanol and 0.1enzymatic unit beta-galactosidase.

Different concentrations of nanoparticle solutions were used with the enzymatic assay in order to study enzymatic release of rhodamine 6G from rhodamine 6G-loaded lactose capped MSNs. Thus, the above assay was incubated with loaded lactose MSN concentrations of 10 mg, 20 mg and 50 mg per 3 ml assay. In another set, the particle concentration was kept at 50 mg and the enzyme concentration varied from 0.1 enzymatic units to 1, 10 and 100 enzymatic unit per 3 ml assay mixture. The release of the dye was monitored spectroscopically at 529 nm.

2.20. Bacterial Biofilm Studies:

The bacterial biofilm was grown on 2 ml -glass petridishes in minimal davis media with 20% dimethyl sulphoxide (DMSO) and 0.5% tween 20. Spectral confocal analysis was performed on the following samples:

- (Control) Biofilm without oil or fluorescent MSN
- Biofilm doped with 625 mg/L of AITC
- Biofilm doped with fluorescent MSN (1mg/mL)

For confocal imaging of the biofilm, the media was removed and the cells were stained with two dyes (2 μg/ml of each dye) - green syto 9 (ex: 488nm; em: 500nm) that dyes both live and dead cells and red propidium iodide (ex: 488nm; em: 635nm) which dyes only the dead cells. Before imaging, the cells were washed with PBS.

3. NANOPARTICLE GENERATION (SYNTHESIS) AND CHARACTERISATION

3.1. Introduction:

The preparation and characterisation of silica and mesoporous silica is discussed. As previously discussed in the Introduction chapter, silica nanoparticles are prepared by the hydrolysis and condensation of tetraethylorthosilicate (TEOS) in the presence of a base (ammonium hydroxide). Thereafter, mesoporous silica nanoparticles (MSN) are synthesised using a similar procedure, employing cetyltrimethylammomium bromide (CTAB) as a template for mesopore formation. The nanoparticles can be functionalised with various groups including aminopropyl, polyethyleneglycol (PEG) or carboxyl which can be either co-condensed with TEOS during the formation of silica nano-sol or postgrafted onto the silica surface after MSN preparation. In the present work, aminopropyl (APTES)-modified MSNs (*via* co-condensation) are coupled with lactose to produce biocompatible MSN delivery vehicles (Figure 3.1).

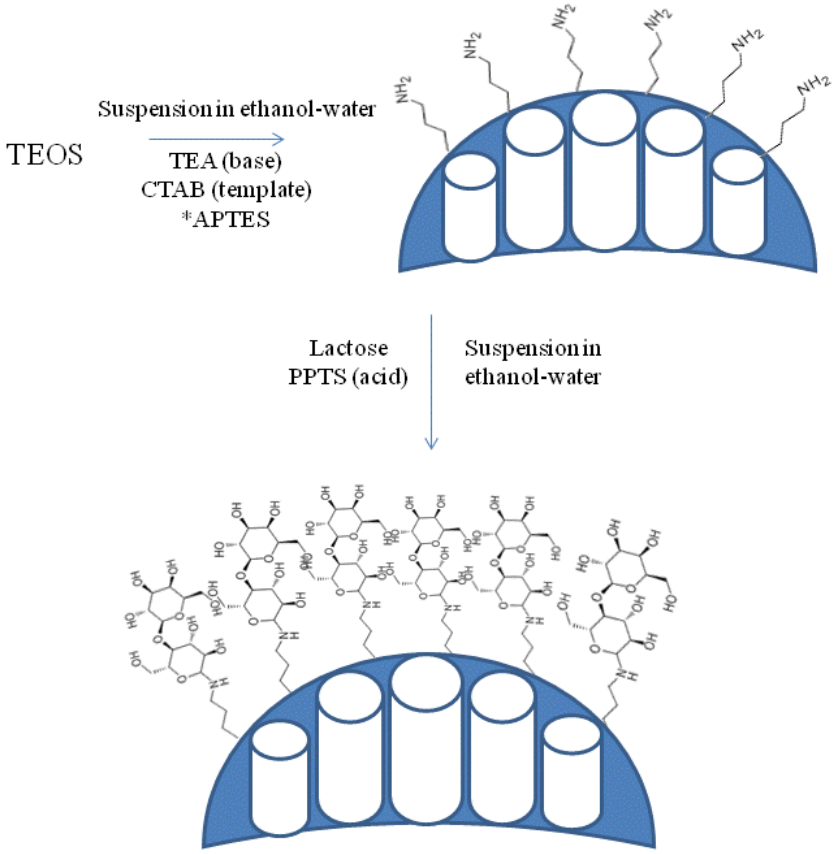

Figure 3.1: Schematic showing the formation of amine-modified MSNs (*via* co-condensation of APTES with TEOS, Experimental chapter) and the proposed lactose coupling to the amine groups on the MSN surface.

3.2. Aims:

This chapter deals with the generation of native, aminated, pegylated and lactose modified MSNs. The efficacy of surface modification with these groups and its effects on colloidal stability would then be discussed. Oil/dye-loaded and lactose capped MSNs would also be characterised to assess their colloidal stability for bacterial cell studies.

The synthesis of silica[21] and mesoporous silica[47] nanoparticles would be carried out as discussed in the Introduction and Experimental chapters. They would then be characterised to

determine their morphology, size, surface functionality, colloidal stability and surface area. The hydrodynamic diameter and polydispersity index (PDI), an indicator of the state of aggregation of MSNs in solution would be determined using dynamic light scattering (DLS). The change in surface charge after functionalisation with amine, carboxyl, PEG and lactose would be studied using zeta potential. Thereafter, Transmission Electron Microscopy (TEM) would be carried out to ascertain the shape, homogeneity and size of the prepared particles. The effect of heating on the morphology of MSNs would be studied *via* TEM. Nitrogen adsorption-desorption isotherms would be used to determine the porosity and surface area of the prepared mesoporous silica. The presence of different functionalities would be analysed by studying the weight loss on thermal degradation using the thermogravimetric analysis (TGA). Infrared spectroscopy would be used to confirm the change in functionalities after each coupling reaction. Finally, incubation with HeLa cells would be performed to study internalisation and uptake characteristics of MSNs.

3.3 Characterisation of Prepared Nanoparticles:

3.3.1. Solubility, Size, Surface Charge and Morphology

The silica nanoparticles and their mesoporous derivatives were synthesised as described in the Experimental chapter. The nonporous silica nanoparticles and MSNs were stable in water and ethanolic solution with concentrations of up to 25 mg/ml. Aminated MSNs with a 1:10 ratio of APTES: TEOS were also found to remain solubilised in ethanolic solution with concentrations up to 30 mg/ml over a month.

The hydrodynamic diameter gives an indicator of nanoparticles size in ethanolic suspensions. PDI was used to describe the width of the particle size distribution, an indicator of the state of aggregation. The data obtained from this study was reproducible with each set of particles prepared (Table 3.1).

Zeta potential measurements allowed measurement of the nanoparticles' surface charge which can vary depending on the functional group attached on the surface. The zeta potential was observed to be negative for plain mesoporous silica nanoparticles and positive for 10% aminated MSNs due to the acidity and basicity of the hydroxyl groups and amine groups respectively on each [56, 100, 101]. The zeta potential for 5% aminated MSNs (Table 3.1) is seen to have a low negative value, indicating partial amination of the silica surface. The zeta potential for carboxylated samples was higher than unfunctionalised MSNs (Table 3.1) due to the higher acidity of carboxylic acid groups compared to hydroxyl groups.

Zeta potential was also employed to study the lactose capping reaction by monitoring the change in potential after the attachment of lactose molecule. For lactose, the zeta potential was expected to range from 0±5mV due to low acidity of the hydroxyl groups on the lactose molecule. Lactose was initially reacted with APTES-MSNs without the assistance of a catalyst as discussed in the Experimental chapter. However, as monitored on the zeta potential, the surface charge was seen to vary from +10-25mV, a value closer to that of APTES-MSNs (+33 mV as expected). Increasing the concentration of lactose in the experiment to a ration of 1:10 APTES: lactose as well as heating the system up to 60°C, use of phosphate buffer for carrying out the reaction and increasing the reaction time, all gave

inconsistent zeta potential values ranging from +15-25mV. Therefore, a second method was employed, which involved preparation of a lactose-APTES moiety followed by post-grafting onto MSNs. However, this technique yielded nanoparticles with a very high degree of aggregation. These particles were unstable and could not be redispersed in ethanol or water. A study by Bernados *et. al* [66] on lactose-APTES MSNs reported the formation of a lactose-APTES derivative for post-grafting onto mesoporous silica supports. This lactose-APTES coupling reaction was carried out entirely in ethanol (in an inert atmosphere) even though lactose is inherently insoluble in ethanol. As reported earlier by our studies, post-grafting reaction led to a high degree of aggregation and hence was unsuitable for mesoporous silica nanoparticle systems where uniformity, degree of aggregation and solubility are vital.

From the zeta potential data discussed above, it was clear that the lactose coupling onto APTES was not consistent. This is likely to be due to the difficulties in the formation of the lactose-amine linkage. This is hindered due to immobilised terminal amine groups on the surface of nanoparticles preventing access. Thus, the reactivity of the lactose group was increased by catalysing its ring opening in the presence of an acid. Careful choice of acid was required, to ensure that it was strong enough to facilitate the ring opening but did not protonate the amine groups on the silica surface. Thus the use of pyridinium para-toluene sulphonate (PPTS) as an acid was considered. The concentration of PPTS was taken in 1:10 ratio of PPTS: APTES. The zeta potential for lactose- MSNs prepared using PPTS was seen to vary between 0±3 mV (Table 3.1). These particles remained suspended in water and ethanolic solutions for up to a week at concentrations of 10 mg/ml. These results indicated successful lactose coupling.

The mesoporous silica nanoparticles were then loaded with oil (allyl isothiocyanate) or dye (rhodamine 6G) and subsequently capped with lactose for antibacterial studies (discussed in Chapter 4). The zeta potential measurements of the lactose capped loaded MSNs was observed to be similar to unloaded lactose capped MSNs, an indication that there was no surface adsorption of the loaded molecules. The values are tabulated below (Table 3.1) after carrying out at least 3-5 measurements for each.

Table 3.1: Size and surface properties of prepared nanoparticles

Particle	Hydrodynamic diameter (nm)	Zeta potential (mV)	PDI	TEM diameter (nm)
Nonporous silica nanoparticles (SNP)	195±5	-39 ± 2	0.10	
Fluorescent SNP	200±5		0.08	
Mesoporous silica nanoparticles (MSN)	134±4	-22 ± 3†	0.08	55-75
5% APTES-MSN	149±4	-12±3	0.07	
10% APTES-MSN	144±4	33 ± 4†	0.10	55-75
Fluorescent MSN	145±5		0.09	
COOH-MSN	145±4	-29± 3	0.04	
PEG-MSN	170±3	-20 ± 3	0.08	
Lactose- MSN	145± 5	0 ± 3	0.09	60-80
Rhodamine 6G- Lactose MSN	160± 3	2± 2	0.12	65-80
AITC-Lactose MSN	140± 4	1± 2	0.22	65-80

†- comparable with literature [5, 100, 101]

The particles were characterised further using transmission electron microscopy (TEM) to determine the exact diameter and the homogeneity of the nanoparticles. TEM of mesoporous silica nanoparticles showed homogeneous spherical nanoparticles with mesopores ranging

from 3-5 nm. The particle size was seen to vary from 55 to 80 nm for the MSNs (Table 3.1) which is similar to literature [47].

(A) *MSNs*: From the images below (Figure 3.2), it was determined that the MSNs were homogeneous and spherical in shape. The particle size ranged from 65±10 nm with mesopores 3-5 nm.

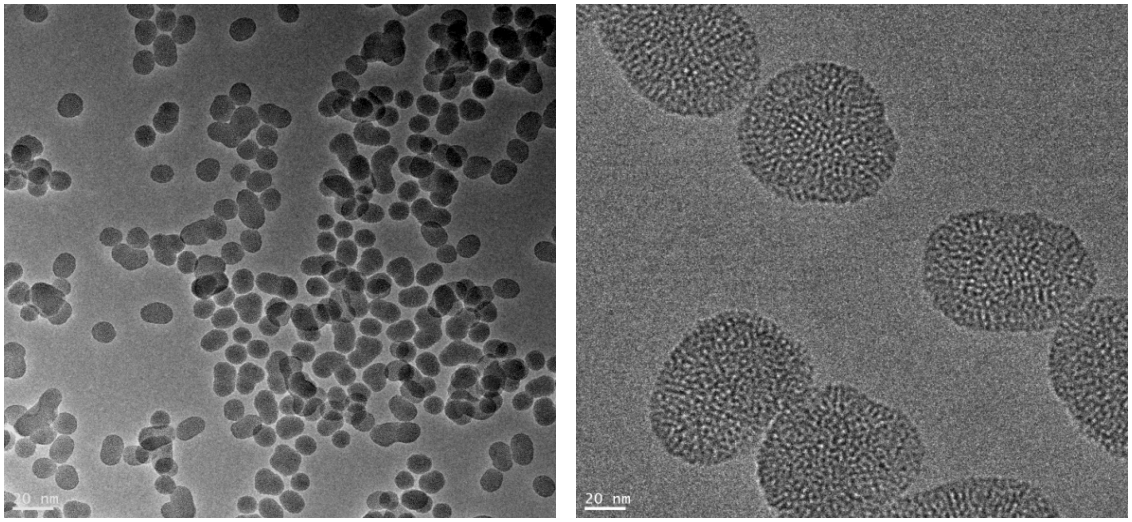

Figure 3.2: TEM images showing homogeneous MSNs with diameters of 65±10 nm.

(B) *APTES-MSNs*: The aminated MSNs were homogeneous with mesopores of 3-5 nm (Figure 3.3). The particle size ranged from 65±10 nm. These particles were subjected to heat treatment at 80°C for 10 hours to study changes in morphology. This was carried out since partial etching was observed for loaded lactose capped MSNs as discussed later. Etching of all particles was observed at the above conditions due to the pore enlargement during this process (Figure 3.4).

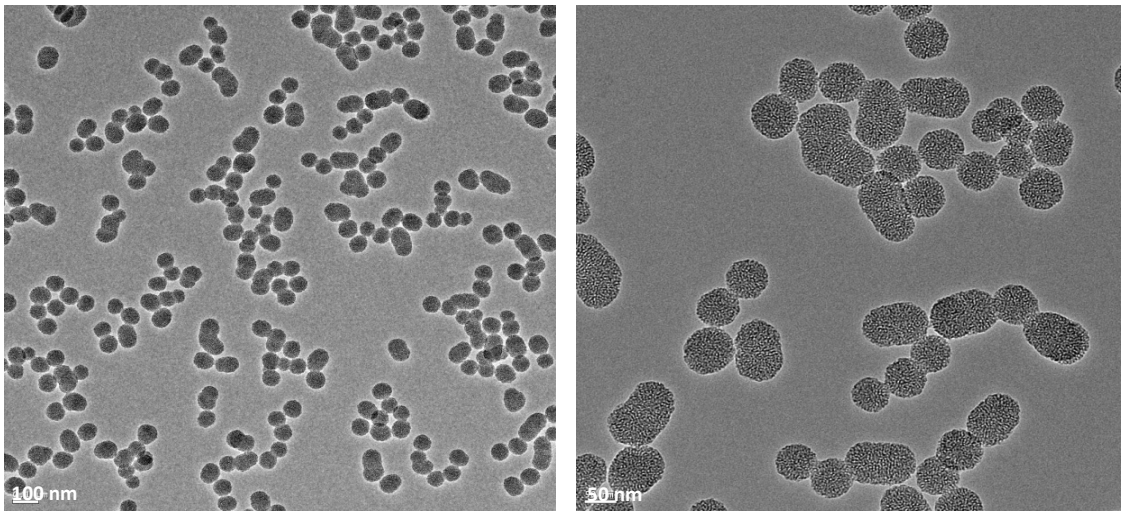

Figure 3.3: TEM images showing aminated MSNs with diameters of 65±10 nm before application of heat.

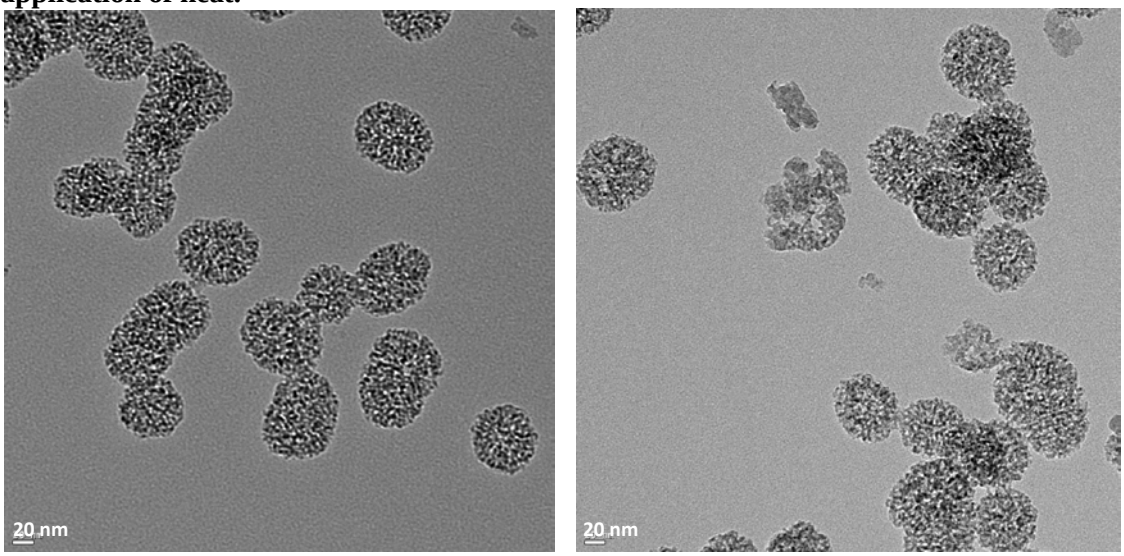

Figure 3.4: TEM images showing change in morphology of aminated MSNs on heating.

(C) *Lactose-MSNs*: The images (Figure 3.5) show uniformity of MSNs after lactose coupling. The particle size varied from 60-80 nm and the presence of mesopores was observable from the TEM images.

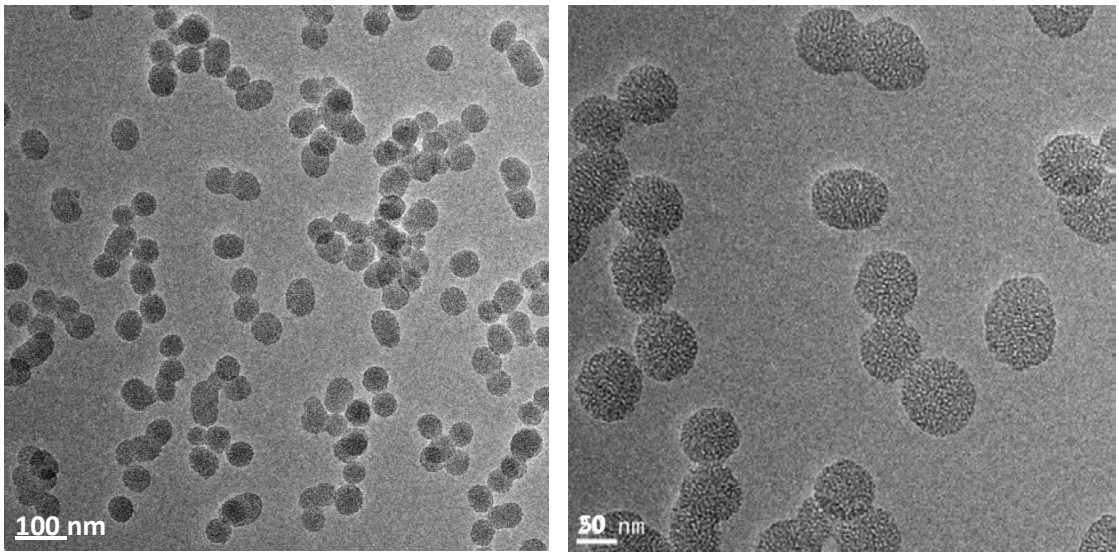

Figure 3.5: TEM images showing homogeneous lactose-MSNs with diameters from 60-80 nm.

(D) *Rhodamine-lactose MSNs*: Observation of rhodamine loaded lactose capped MSNs showed the overall particle morphology as spherical (Figure 3.6). However, there was slight aggregation as observed from the images. Some particles are seen to be etched due to heat generated during sonication (up to 70°C). From these images, the size is seen to vary from 65-80 nm.

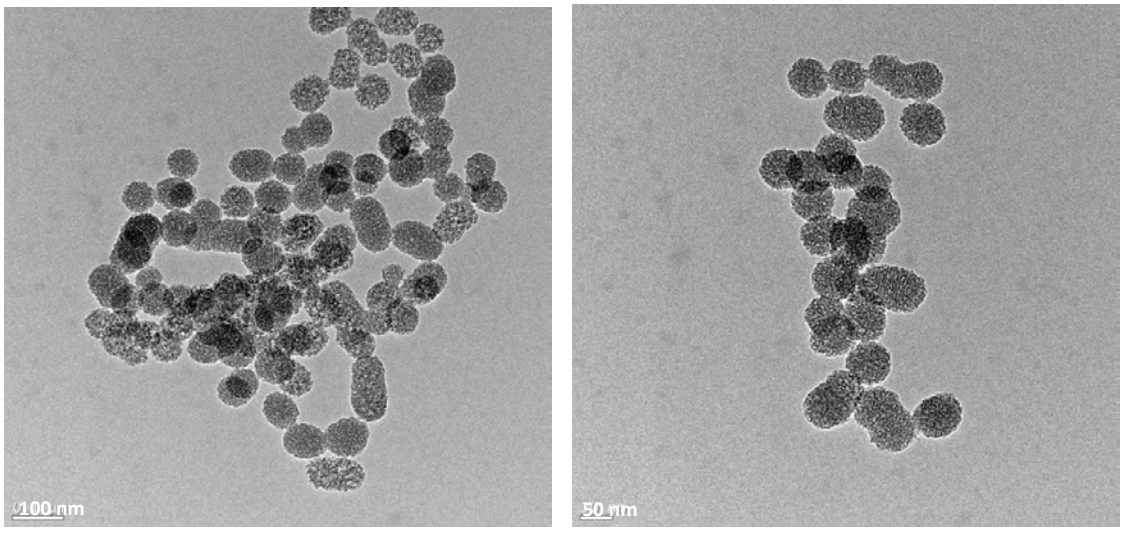

Figure 3.6: TEM images showing rhodamine loaded lactose-MSNs with diameters from 60-80 nm with partial etching.

(E) *AITC-Lactose MSNs*: The images of allylisothiocyanate loaded and lactose capped MSNs showed similar morphology to the rhodamine lactose MSNs (Figure 3.7). Slight aggregation supported by increase in PDI and partial etching was observed in these as well with the size varying from 65-80 nm. As previously mentioned, apparent etching was thought to be caused by pore enlargement due to heating.

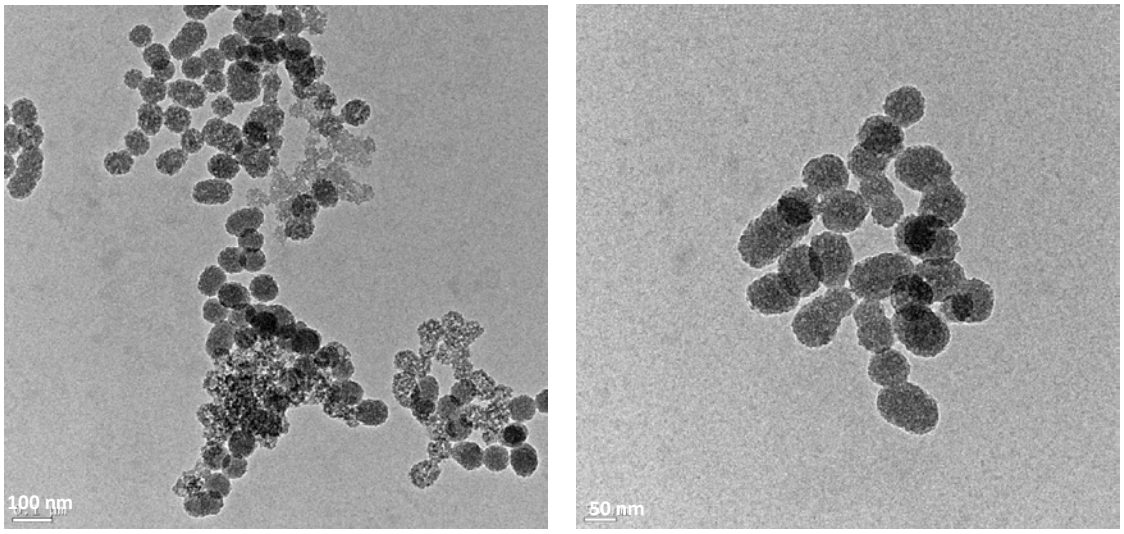

Figure 3.7: TEM images showing AITC loaded lactose-MSNs with diameters from 60-80 nm with partial etching.

Thus, the TEM images showed homogeneous spherical MSNs with sizes ranging from 55-80 nm (Table 1). The presence of mesopores was observed from these images which varied from 3-5 nm. The exact size of the mesopores was calculated from nitrogen adsorption-desorption experiments.

3.3.2. Porosity and Surface Area

Nitrogen adsorption-desorption experiments were carried out with aminated MSNs (since these MSNs were used for loading-release experiments and for lactose coupling). The specific surface area, pore volume and pore size were calculated from these measurements (Table 3.2).

They were found to be similar to literature [47, 48, 102]. The pore diameter was in accordance with those observed *via* TEM and published results.

The adsorption data was plotted as pore radius to volume graph to show the range in which adsorption occurred in the MSNs. It was observed that 70% of nitrogen adsorption took place up to a radius of 1.8 nm (Figure 3.8) indicating adsorption in the mesopores of the MSNs. Thus, the mesopore diameter was calculated as 3.6 nm. The remaining 30% of adsorption took place between 110-1000 nm, indicating surface adsorption.

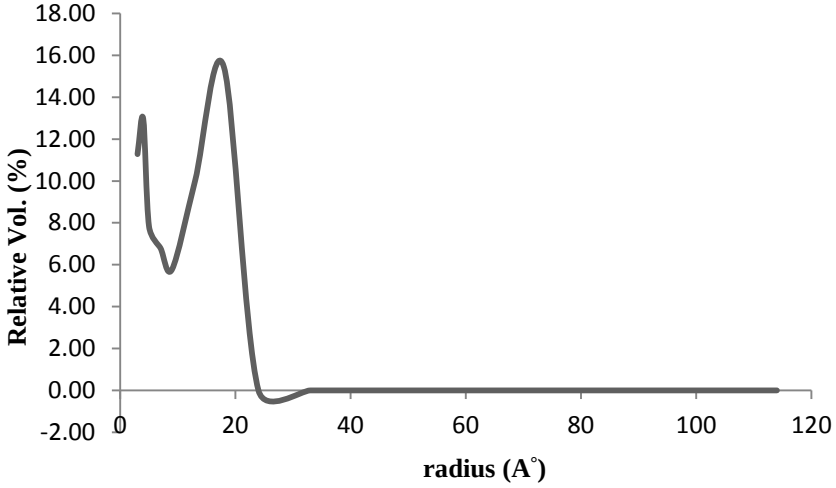

Figure 3.8: Pore size distribution graph of volume vs radius indicating nitrogen adsorption inside mesopores of radii 1.8 nm.

Table 3.2: Adsorption data showing specific surface area, pore volume and pore diameter obtained for aminated MSNs.

Specific surface area (m^2/g):	**901.1 ± 4.5**
Pore specific volume (cm^3/g):	0.98 ± 0.04
Pore diameter (nm):	3.6

The nitrogen adsorption-desorption data could not be performed with loaded lactose capped MSNs due to the degradation of lactose at 200˚C. For the adsorption studies, complete removal of water molecules is needed for which the sample is to be heated and degassed at a

minimum of 200°C for 10-12 hours. Thus, degradation of lactose under these conditions would result in unreliable results for these particles.

3.3.3. Thermal Degradation Studies

The purity of the particles and presence of functionalities on silica were determined using thermo gravimetric analysis by monitoring the weight loss with increasing temperature.

(A) *MSNs*: Correlating the observed graph for unfunctionalised MSNs to literature[48] (Figure 3.10), a weight loss of 5% at 100°C was seen indicating the loss was due to water (Figure 3.9). The loss due to hydrocarbons at 250°C was 1% by weight observed *via* derivative plots (not shown here) indicating most of the CTAB used as a template during mesoporous particle formation was successfully removed. It was also concluded that silica nanoparticles were thermally stable up to 600°C.

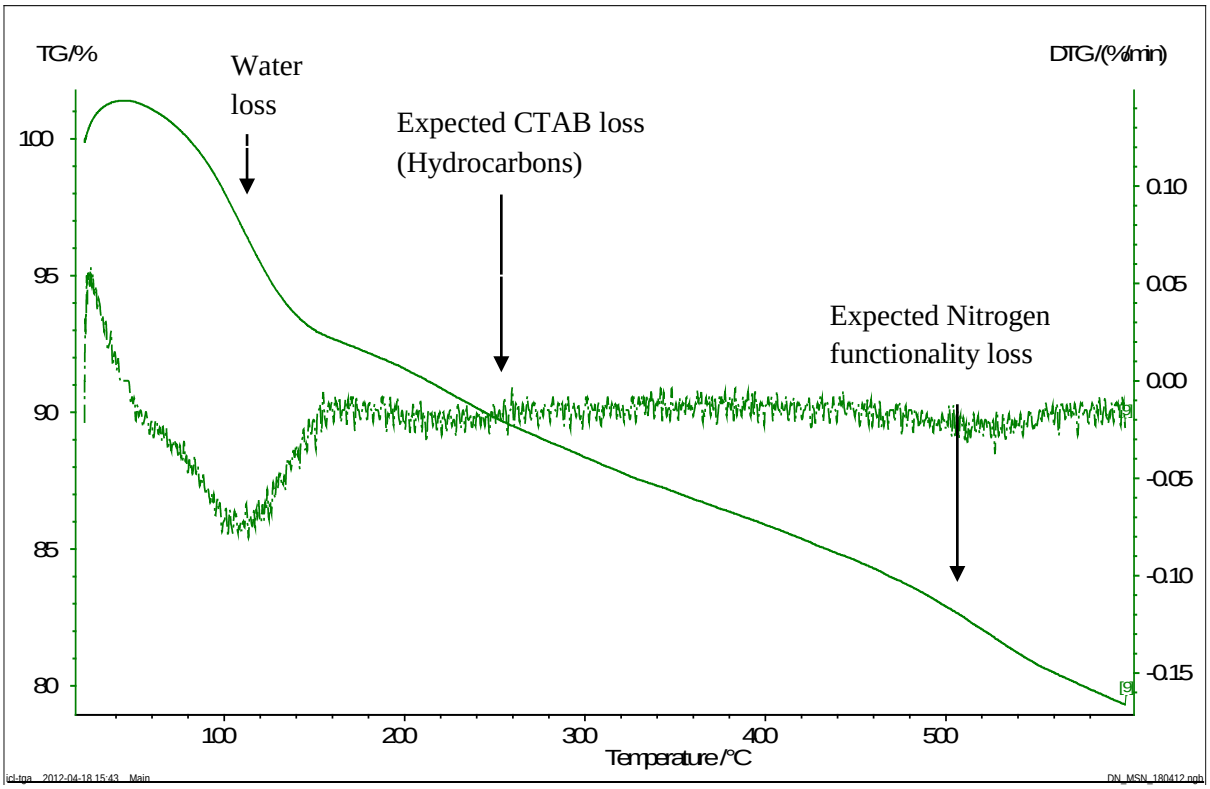

Figure 3.9: TGA for unfunctionalised MSNs after template removal showing weight loss due to water (7%), hydrocarbons like CTAB (1%) and nitrogen moiety due to CTAB (0.5%) at 100˚C, 250˚C and 550˚C respectively.

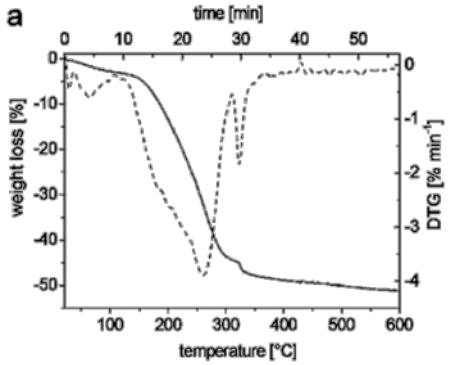

Figure 3.10: TGA curve reproduced from Kobler *et.al*, ACS Nano, 2008, 2, 791-799.

TGA studies were employed to study the presence of oil loading within the mesopores of lactose capped MSNs. The TGA curves for unloaded lactose MSNs are compared with AITC loaded lactose capped MSNs to determine AITC loaded.

(B) *Lactose-MSNs*: The TGA curve for Lactose MSN showed a 5% weight loss due to water, and a 3% weight loss for hydrocarbons between 250-300˚C. A weight loss of 1% was seen at 550˚C indicating the thermal degradation of the aminopropyl chain.

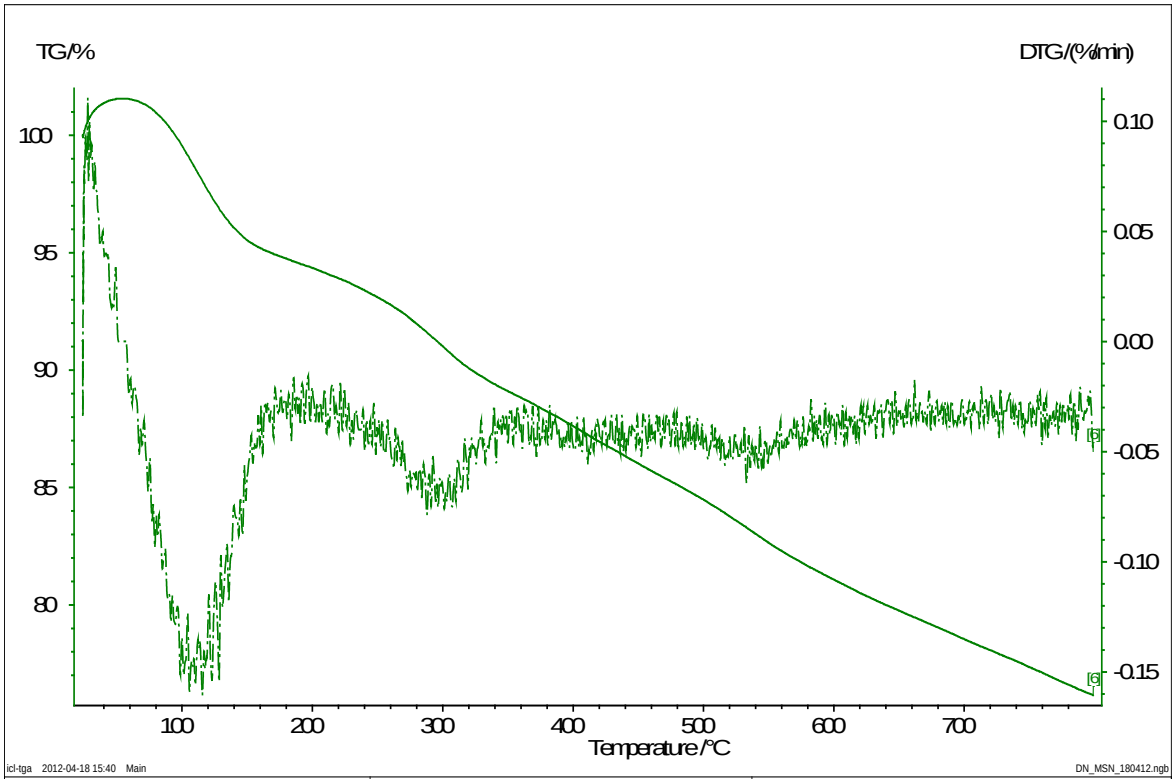

Figure 3.11: TGA for lactose MSNs showing weight loss due to water (5%), hydrocarbons like lactose (5%) and nitrogen moiety due to the aminopropyl chain (1%) at 100˚C, 250˚C and 550˚C respectively.

(C) *AITC-Lactose MSNs*: TGA curve for allylisothiocyanate loaded Lactose MSN had a weight loss of 2% for water, 5% for hydrocarbons and another 5% around 550˚C for the propyl chain and allylisothiocyanate. Thus, from this curve, it was concluded that a loading of 5% had been achieved in the mesopores of the mesoporous nanoparticles.

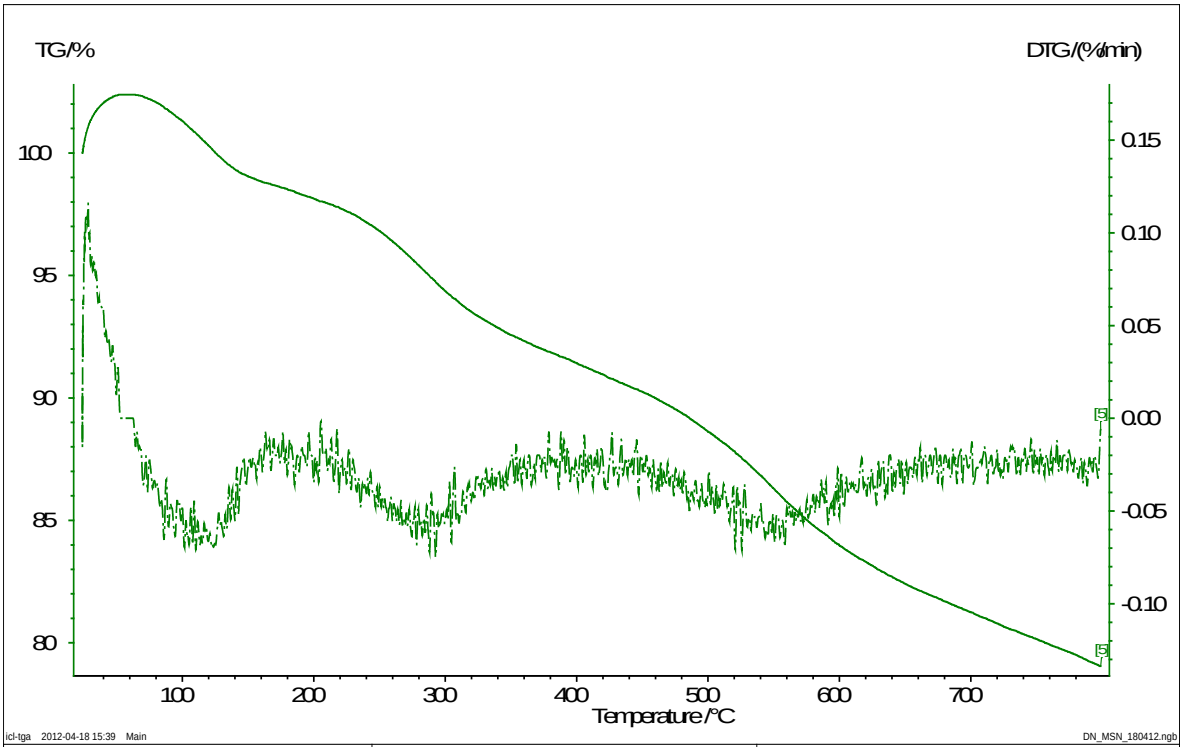

Figure 3.12: TGA for AITC loaded lactose MSNs showing weight loss due to water (2%), hydrocarbons like lactose (6%) and nitrogen moiety due to the aminopropyl chain and AITC (5%) at 100˚C, 250˚C and 550˚C respectively.

3.3.4. Presence of Functionalities via Infrared Spectroscopic Studies

Infrared spectroscopy was performed to study the presence of primary amine functionality and the change after lactose coupling (See Appendix).

The IR spectra of unfunctionalised mesoporous silica had a very strong peak and shoulder at 1110 cm^{-1} associated with the stretching vibrations of Si-O-Si network. A strong, broad peak between 3200-3500 cm^{-1} indicative of the O-H stretching (and hydrogen bonding) of the silanol group is observed. As determined from TGA, 1% residual CTAB by weight was

present in the unfunctionalised MSN samples that gave small signals at 2900 cm^{-1} (C-H stretch from CTAB) and 1650 cm^{-1} (N-H bend from CTAB) on the FTIR.

The IR spectra for aminated MSN, showed a medium peak at 1600 cm^{-1} indicating N-H stretching by primary amines. An overlap of N-H stretching and O-H stretching in 3200-3500 cm^{-1} range was observed. However, the presence of two bands in this region for primary amines was detected. These stretches are summarised in table 3.3.

Table 3.3: List of FTIR absorption frequencies observed for MSN samples:

Frequency (cm^{-1})	**Type of vibration**	**Intensity**	**Functional group**
1110	Stretch	Very Strong	Si-O-Si
1580-1650	Bending	Medium	N-H
2850-3000	Stretch	Strong	C-H
3200-3500	Stretch, H-bonded	Strong, broad	O-H
3300-3500	Stretch	Medium (2 bands for primary amines, 1 very weak band for secondary amines)	N-H

In the IR spectra for Lactose- MSN, lowering in intensity of N-H stretch at 1600 cm^{-1} was seen due to reaction of amine groups with lactose and thus the conversion of primary amines to secondary amines. The two bands in the 3200-3500 cm^{-1} range due to primary amines were not observed. Instead a weak band at 3200 cm^{-1} is seen that is due to the O-H stretching from hydroxyl groups on lactose.

Overall, the IR spectra of MSNs showed a strong, broad peak between 3200-3500 cm^{-1} due to the O-H stretching of the silanol groups. A small signal for CTAB was observed due to the C-H stretching and N-H bending at 2900 cm^{-1} and 1650 cm^{-1} respectively. The successful amination of the MSNs was observed by the medium peak at 1600 cm^{-1} showed by primary amines (N-H stretch). The presence of two bands in the 3200-3500 cm^{-1} range for primary amines was also detected. The conversion of primary amines to secondary amines on lactose coupling was determined by a decrease in the N-H stretch at 1600 cm^{-1} and the absence of two bands in the 3200-3500 cm^{-1} region. Instead a single broad band at 3200-3500 cm^{-1} was observed due to the hydroxyl groups on lactose molecules.

3.4. Hela Cell- Nanoparticle Incubation Studies:

Incubation of fluorescent MSNs (f-MSNs) and fluorescent pegylated MSNs with Hela cells was carried out to study the internalisation and uptake characteristics of f-MSN nanoparticles in these cells. Concentrations of 0.1 mg/ml were used for incubation and it was seen that the f-MSNs were internalised within 3 hours of incubation. The cells were then treated with the same concentration of pegylated f-MSN. It was observed that the nanoparticles were being up taken only after 30 hours of incubation indicating that pegylation delayed the uptake of MSNs in Hela cells.

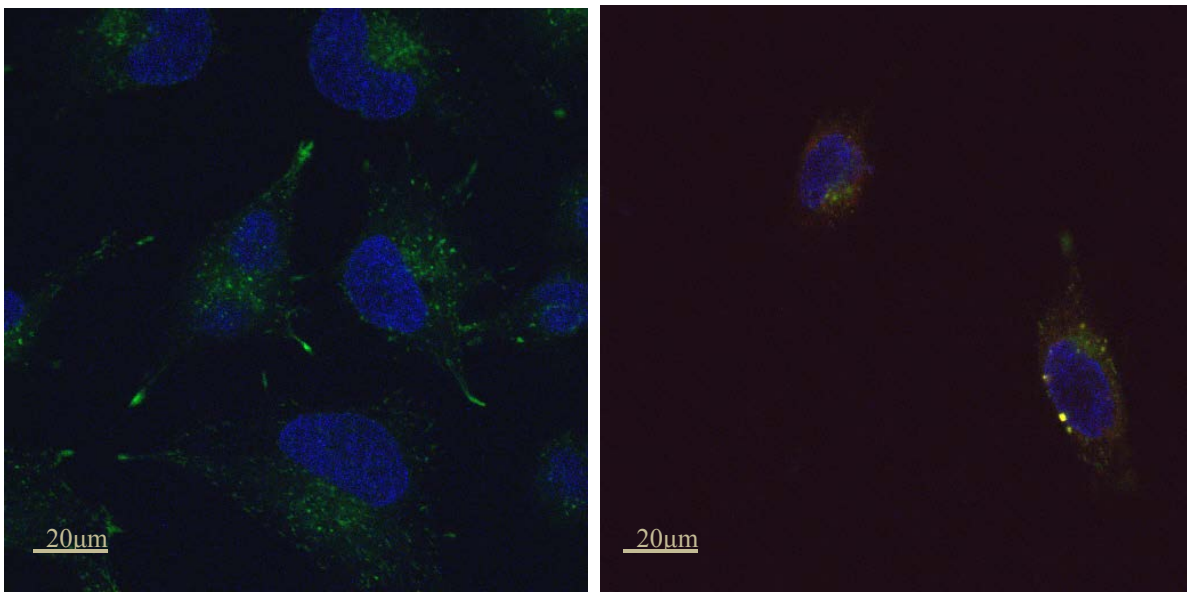

Figure 3.13: Hela Cells with f-MSNs: The first image shows Hela cells dyed with green lysosome dye (Lysotracker Green DND-26) and blue nuclear dye (Hoechst 33342). The second image shows the yellow overlap of green lysosome dye with red f-MSN after 3 hours of incubation indicating their internalisation.

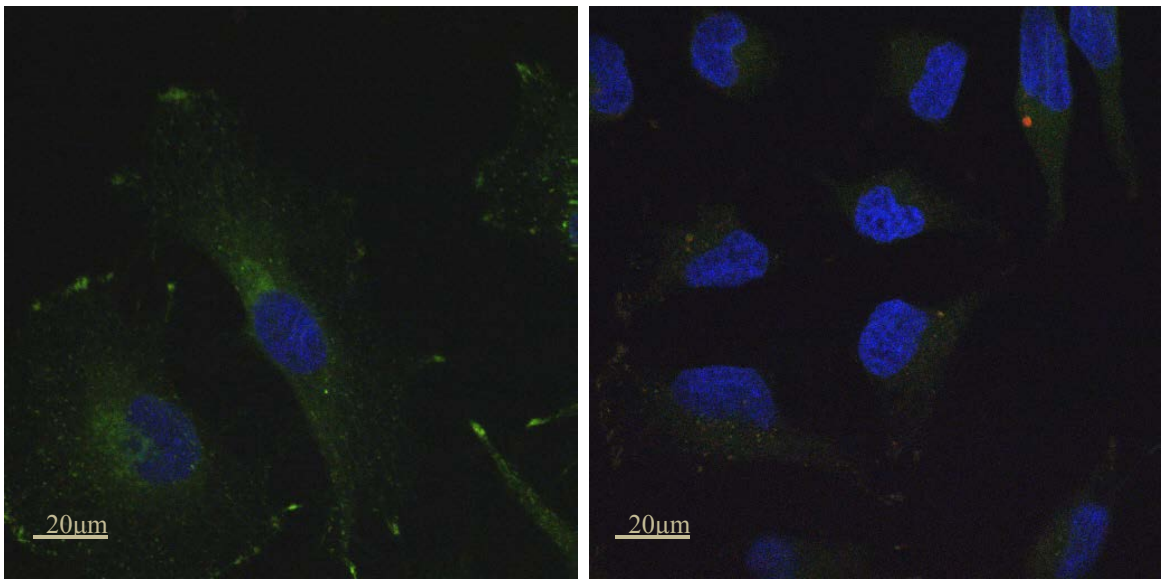

Figure 3.14: Hela cells with PEG-MSNs: After incubation of Hela cells with pegylated MSNs, no uptake was observed until 30 hours of incubation. The first image was taken after 3 hours of incubation. The second image shows a an overlap of green and red dye indicating that the particles were being up taken after 30 hours.

3.5. Conclusions:

The MSNs were successfully prepared and fully characterised using DLS, Zeta Potential, TEM, TGA, FTIR and Nitrogen Adsorption-desorption. The MSNs were found to be spherical, homogeneous and colloidally stable in solution with diameters ranging from 55-75 nm and pore sizes of 3.6 nm. On coupling with APTES, the spherical shape, homogeneity and colloidal stability were retained. The porosity and surface area was determined using nitrogen adsorption-desorption isotherms and was found to be similar to literature. The presence of functional groups including APTES and lactose was confirmed using zeta potential, FTIR and TGA. The oil (AITC) loaded and lactose capped particles were seen to be homogeneous though with a slight degree of aggregation confirmed by PDI and TEM images. The presence of oil loaded inside the mesopores of the capped MSNs was determined to be 5% by weight on the TGA. Finally, incubation of f-MSNs and PEG-MSNs with HeLa cells was performed to confirm internalisation and uptake time within the lysosomes of the HeLa cells with doses of 0.1 mg/ml for f-MSNs and pegylated f-MSNs. Internalisation of f-MSNs took place within 3 hours of incubation. However, PEG-MSNs were internalised only after 30 hours of incubation indicating that the PEG chain contributed to longer circulation and delayed internalisation of MSNs inside the lysosomes of HeLa cells.

4. MSNs AS ANTIBACTERIAL AGENTS

4.1. Introduction:

Mesoporous silica nanoparticles can be envisaged as delivery vehicles for naturally occurring antibacterial oils. These oils are hydrophobic and volatile which limits their efficacy and toxicity against bacterial cells. MSNs were successfully synthesised as discussed in the previous chapter. They were homogeneous and colloidally stable for use as hosts for antibacterial agents. Due to the highly porous nature of MSNs, their use as an uptake and delivery system is highly advantageous. Here, an MSN delivery system is studied which encapsulates the oils and provides controlled and targeted delivery of these oils to the bacterial cells. Since the bacterium of study in this project is *Escherichia coli*, lactose was chosen as the capping agent due to its nontoxicity and enzymatic hydrolysis by beta-galactosidase produced by these bacterial cells. It is expected that the killing efficiency would be higher for these nanoparticles due to the encapsulation of the oil within the mesopores and the hydrophilicity of the MSNs.

4.2. Aims:

In this chapter the application of synthesised MSNs as antibacterial agents is discussed. Mesoporous silica nanoparticles would be doped with antibacterial agents in order to investigate their loading and release capacity and rate as well as their capability as antibacterial vehicles. Specifically, the MIC dosage of the oils would be determined by following the cell growth (by monitoring the optical density of the bacterial suspension at 600 nm) for different concentrations of the oil. Following this, the native toxicity of unloaded

MSNs with *E.coli* bacterial cells was to be studied to determine the maximum nanoparticle concentration that would be suitable for cell studies. Lactose capping studies would then be carried out to study access of water and oils from the capped pores. Gadolinium doped MSNs would be used as Magnetic Resonance Imaging (MRI) contrast agents to study the capping effects of lactose by blocking water access to the pores of the MSNs. Thereafter, loading and release of the two antibacterial oils- allylisothiocyanate (AITC) and cinnamaldehyde was to be carried out using different concentrations to determine the maximum loading that can be achieved. As a reference, the loading and release studies would be repeated with a dye rhodamine 6G. Release *via* enzymatic hydrolysis of lactose would be conducted using the commercial enzyme beta-galactosidase. Finally, incubation of oil loaded lactose MSNs with bacterial cells shall be studied to investigate antibacterial effects *via* cell viability assays.

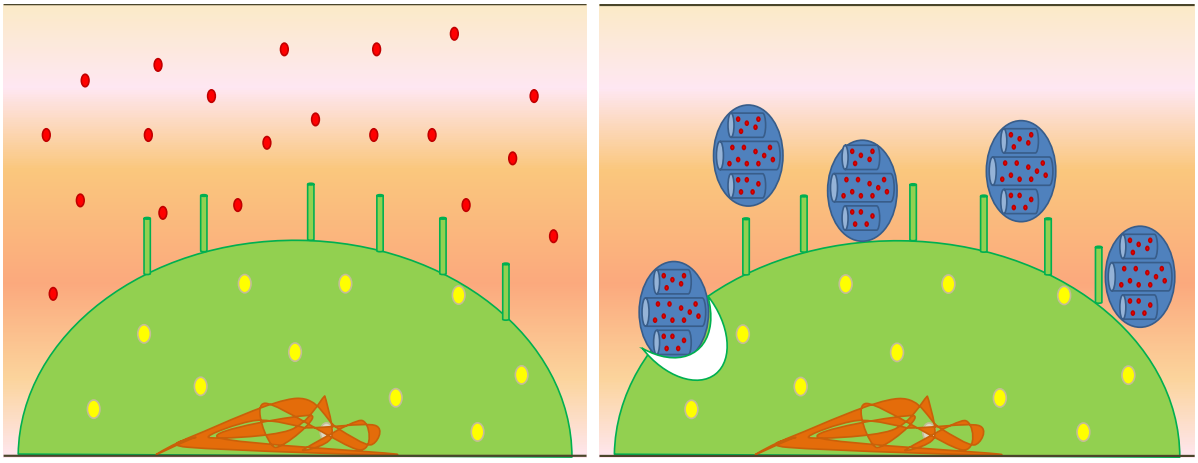

Figure 4.1: Schematic showing the expected bacterial interactions with the oils and nanoparticles: (left) showing the oil (red) in the bacterial suspension (depicted in green with yellow ribosomes and orange nucleoid in the cytoplasm). As the oils are volatile and hydrophobic, they remain in suspension and do not efficiently cause bacterial cell death; (right) shows the oil-encapsulated nanoparticle that is expected to be readily ingested by the bacterial cell. It is hoped that the nanoparticle system presents an easier and more efficient delivery of the antibacterial oil to the bacterial cell in markedly lower doses than the pure oil.

4.3. Oil Toxicity Studies:

The toxic dosage of the oils required for antibacterial activity was determined by the microdilution test (Figure 4.2). In this experiment, a single bacterial species was treated with oil concentrations ranging from 2500mg/L to 9.77mg/L. The cells were studied in 200 µl measuring 96- microwell plates (see experimental section) and studied by measuring optical density OD600 for the bacterial suspensions, which is an indicator of cell growth [99]. The minimum inhibitory concentration (MIC) - lowest concentration of a substance that inhibits visible growth was then calculated from this experiment (with at least 3 sets each) and was found for *E.coli* cells as:

AITC: 625mg/L; 6.3mM

Cinnamaldehyde: 312.5mg/L; 2.36mM

This is the toxic dosage that needs to be delivered from silica nanoparticles for satisfactory antibacterial activity. Comparing the MIC to published literature (Introduction chapter) the values determined for AITC are nearly 20 times higher. This may be attributed to the volatility of the oil. The dosage for cinnamaldehyde is comparable to published results.

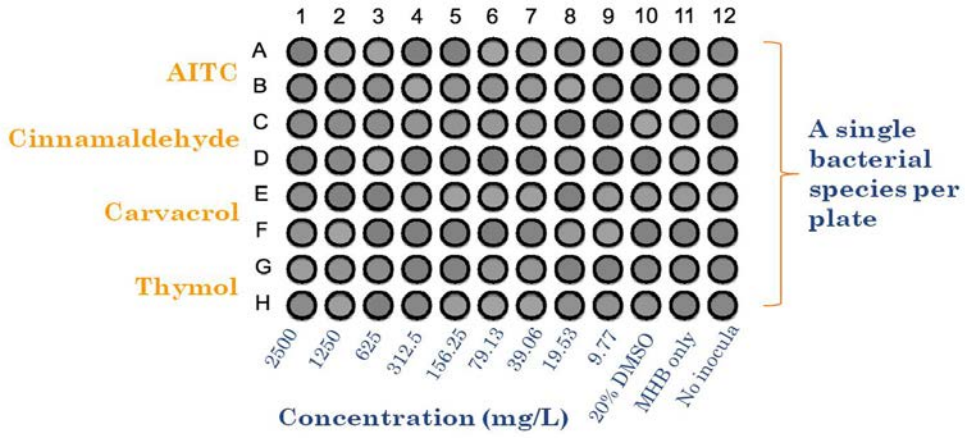

Figure 4.2: Set-up to study the toxicity of oil with bacterial species : Each circle represents a 200 µl microwell containing the bacterial suspension treated with antibacterial oils with

concentrations from 2500 mg/L to 9.77 mg/L. The cell growth was monitored spectroscopically at 600 nm over 18 hours.

4.4. Nanoparticle Toxicity Studies:

Since lactose is proposed as the capping agent, the inherent toxicity of lactose coated MSNs is studied here. These toxicity studies were conducted by incubating varying concentrations of MSNs with bacterial suspension. For this purpose, *E.coli* cells were suspended in phosphate buffer and incubated with MSNs (Experimental chapter). The cell growth was studied over 18 hours to determine the cell viability in the presence of nanoparticles. The following data was obtained (each repeated 3 times, Table 4.1).

Table 4.1: Cell viability for *E.coli* cells incubated with 2mg/ml and 5mg/ml Lactose-MSNs in 0.1M phosphate buffer solutions (pH 7.3):

Cells	Viability (live bacteria)
Control with just cells	78.8 ± 5 %
Cells incubated with 2mg/ml MSNs	81.3 ± 5 %
Cells incubated with 5mg/ml MSNs	63.3 ± 6 %

Suspensions with higher cell viability indicate the presence of live healthy cells that are capable of forming bacterial colonies. The viability is observed to be higher for 2mg/ml lactose MSNs which may be due to the availability of lactose on the lactose MSNs as a suitable source of nutrient for *E.coli* cells [91]. On increasing MSN concentrations, the percentage of viable cells is seen to decrease and is an indication of the cytotoxicity of these unloaded nanoparticles. The fluorescent lactose MSNs prepared (experimental section) were imaged on the laser scanning confocal microscope to confirm their internalisation in bacterial cells (see Appendix).

Thus it was concluded that lactose coated MSN suspensions up to 2 mg/ml were non-toxic to *E.coli* bacteria. A suspension with 5 mg/ml concentration of nanoparticles reduced the cell viability by 15-18%.

4.5. Uncapped Oil -loaded Nanoparticle Release:

The MSNs were doped with antibacterial oils- allylisothiocyanate (AITC) and cinnamaldehyde and a dye rhodamine 6G (Experimental chapter) in order to quantify the amount loading and release, as well as rate of release from the mesopores of uncapped nanoparticles. These loading studies were carried out to ascertain the absence of any chemical interaction of the oils other than van der Waal's interaction with either the particles or the solvent. This also gave an indication of the maximum payload that can be released from these nanoparticles.

4.5.1. Allyl isothiocyanate (AITC) and Cinnamaldehyde

The uptake of AITC and cinnamaldehyde into MSNs was conducted with varying concentrations of 1 µl/ml, 10 µl/ml and 50 µl/ml (AITC density: 1.01 g/ml; Cinnamadehyde density: 1.05 g/ml). The release of the oils from the MSNs was monitored spectroscopically at 245 nm and 291 nm respectively (see Appendix for UV-Vis Spectra). As expected, the quantity released was lowest from 1 µl/ml oil solution. However, release from 10 µl/ml AITC solutions was comparable to 50 µl/ml indicating a loading saturation of the mesopores with the oil. This indicates optimised oil uptake of 10 µl/ml. The maximum oil that can be delivered from an uncapped MSN over 24 hours was calculated as 0.058 mg/mg of MSN for

AITC and 0.022 mg/mg of MSN for cinnamaldehyde (Figure 4.3, Table 4.2). This release data is comparable to delivery of vancomycin and ruthenium bipyridyl dye as described earlier (Introduction chapter) [2, 8]. Correlating the maximum delivery of oils from MSNs (Figure 4.3, Table 4.2) to the pure oil MIC dosage obtained from oil toxicity studies reported previously, the concentrations of MSNs required to deliver these doses are calculated as 12 mg/ml and 20 mg/ml of AITC and cinnamaldehyde doped MSNs respectively. These nanoparticles concentrations would be inherently toxic to the cells but is hoped that the oil-encapsulated MSNs would be toxic at markedly lower concentrations that of the pure oil itself.

Controls were carried out with nonporous silica to study adsorption of the oils on the silica surface. It was noted that there was an uptake of 0.002- 0.003 mg/mg of nanoparticle. This is significantly lower than the uptake in MSNs, showing that the maximum oil adsorbed in MSNs was adsorbed in the high surface area of mesoporous channels.

4.5.2. Rhodamine 6G

Loading and release of rhodamine 6G was performed to compare the profiles and performance with the oils. For rhodamine 6G, the absorbance at 529 nm (extinction coefficient of 116,000 M^{-1} cm^{-1}) [103] was followed spectroscopically. The release profiles were studied with concentrations of 1mg/ml and 10 mg/ml. The adsorption in mesopores was lowest for 1 mg/ml solutions. However, the amount adsorbed was significantly lower than the oils, indicating reversible loading of the mesopores and constant diffusion to and from the mesopores due to the difference in viscosity of the oils and the dye.

The maximum amount dye that can be delivered from an uncapped MSN over 24 hours was determined to be 0.012 mg/mg of MSN (Figure 4.3, Table 4.2) which is similar to the release reported in literature- 10 μg per mg of MSN [5].

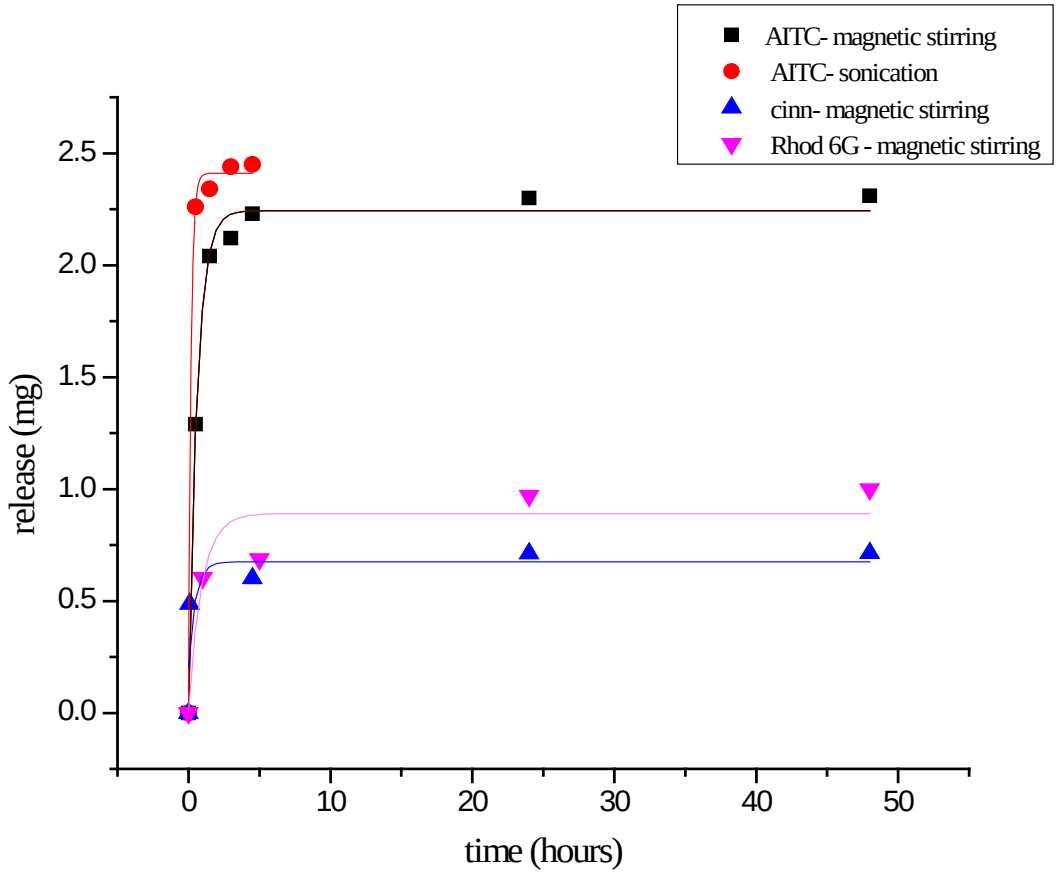

Figure 4.3: Graph showing the release profile for AITC-loaded nanoparticles (40 mg), cinnamaldehyde-loaded nanoparticles (40 mg) and rhodamine 6G-loaded nanoparticles (100 mg) in ethanol. The release curves have been fitted to first-order rate kinetics.

The kinetic rates and maximum release of each doped agent from uncapped MSNs are tabulated in Table 4.2.

Table 4.2: Table showing first-order rate kinetics and maximum release for the oils and rhodamine 6G.

	AITC (sonication)	AITC (stirring)	Cinnamaldehyde (stirring)	Rhodamine 6G (stirring)
Release rate (s^{-1})	5.54	1.66	2.03	1.08
Max. Release per mg of MSN		0.058mg; 0.585μmol	0.022mg; 0.166μmol	0.012mg; 0.025μmol

The release of AITC from an uncapped MSN was compared in two ways *via* magnetic stirring and sonication. As expected, the release rate due to sonication was faster and a higher total percentage of AITC was released (Figure 4.3; Table 4.2). Release due to magnetic stirring was 10% lower than the amount released due to sonication over 24 hours. However, the method of magnetic stirring is preferred in release studies since this method of shaking can be applied to biological entities where these particles would be used.

The release profiles of the oils on magnetic stirring in Figure 4.3 show 60% of the total release occurs during the first 3 hours. The release over 24-48 hours was negligible.

In conclusion, the uptake-release studies from uncapped MSNs gave an indication of the maximum payload release from the mesopores of MSNs (Table 4.2). The release profiles indicated release of the loaded drug/dye in solution and hence capping was required to contain the doped agent in the mesopores until the MSNs reached the targeted species.

4.6. Lactose Coating of MSNs:

Following the release studies of the oils from uncapped MSNs, blocking of the pores with lactose was carried out. The prepared lactose-capped MSNs (Experimental chapter) were

characterised by zeta potential, TGA and FTIR to determine the presence of lactose on the MSN surface as discussed in the previous chapter (Chapter 3). Here, the role of lactose as a cap for the oils and water is discussed.

4.6.1. Release from Oil-loaded Lactose MSNs:

Maximum loading of the MSNs with AITC was carried out according to the optimised procedures described previously and subsequently capped with lactose. From TGA studies (Chapter 3), it was determined that the amount of AITC in lactose-MSNs was 5% by weight i.e. 0.05 mg/mg of MSN which is similar to uncapped loading studies, as expected. The release of the oil or the dye was monitored spectroscopically from lactose capped MSNs and the release was negligible (Figure 4.4) indicating successful retention of the oil in the mesopores by the lactose cap. From figure 4.4, it was seen that less than 0.1 mg of rhodamine 6G or AITC was lost from 40 mg of loaded capped MSNs.

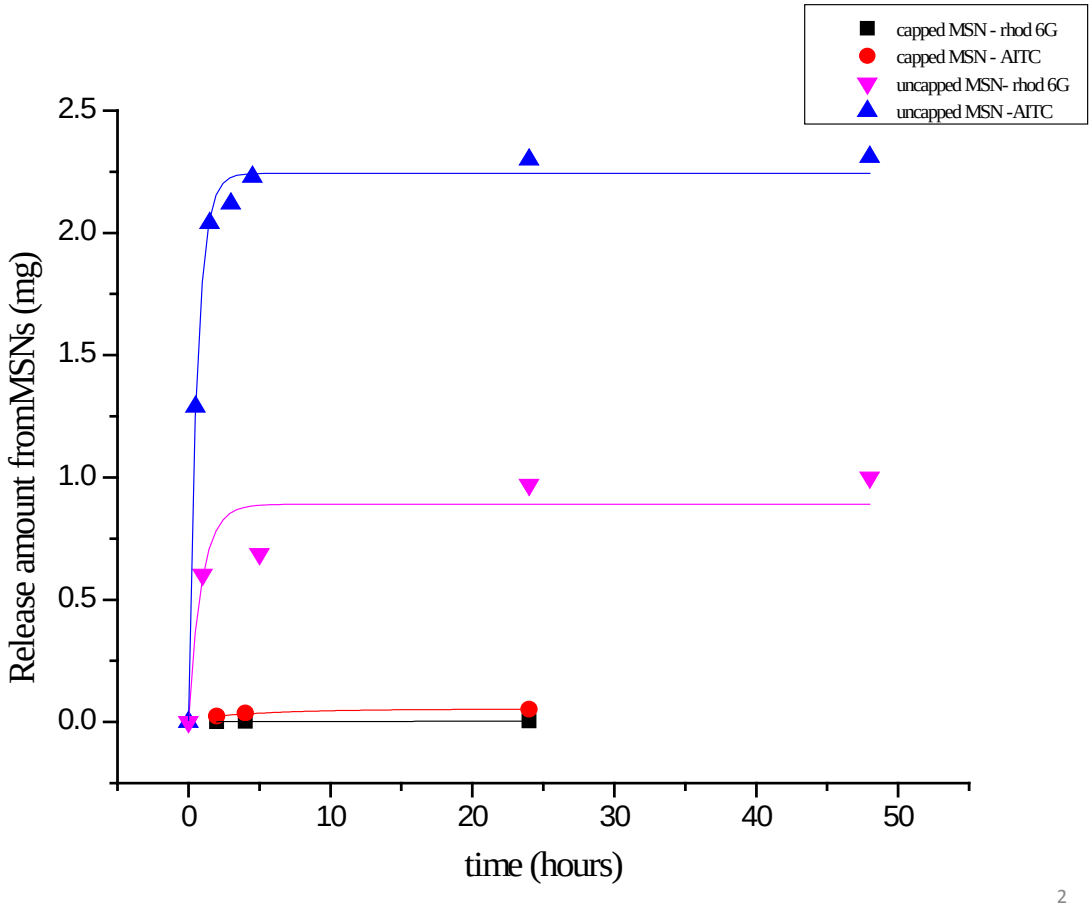

Figure 4.4: Plot to compare the release of AITC and rhodamine from lactose coated MSNs with uncapped MSNs. The maximum amount released over 24 hours was observed as 0.06 µg/mg of MSN for rhodamine 6G and 1.3 µg/mg of MSN for AITC. This amounts to 0.5% and 2.2% of the amount loaded in uncapped MSNs for rhodamine 6G and AITC respectively.

4.6.2. Water Access to Mesopores in Gadolinium Doped Lactose MSNs:

An additional probe of lactose capping efficiency involved Gadolinium (Gd) doped MSNs as Magnetic Resonance Imaging (MRI) contrast agents to study relaxivity - an indication of water access to the mesopores of the MSNs. Contrast agents serve to enhance relaxivity by their interaction with surrounding water molecules. The internal mesoporous surfaces of MSNs were predominantly doped with Gd. Capping these Gd-doped MSNs (Experimental

chapter) with lactose leads to a decrease in water access and hence a decrease in relaxivity is expected, which is indicative of the presence of an effective cap.

MSNs were doped with Gd by covalently chelating it onto aminated MSNs (Experimental chapter). Amine-functionalisation *via* post-grafting was performed to obtain higher doping inside the mesopores. The prepared particles were studied using MRI to determine the decrease in relaxivity indicating low water access to the pores of the Gd doped MSNs (Figure 4.5). The relaxivity for Gd-MSNs as calculated from the graph was 18 mM^{-1} cm^{-1}which is similar to literature [104]. After lactose capping, the relaxivity was seen to decrease by 60-75%. The slopes of the plots give the relaxivity value showing a 75% decrease in relaxivity ($r_1$of 4.09 mM^{-1} cm^{-1}) on lactose capping.

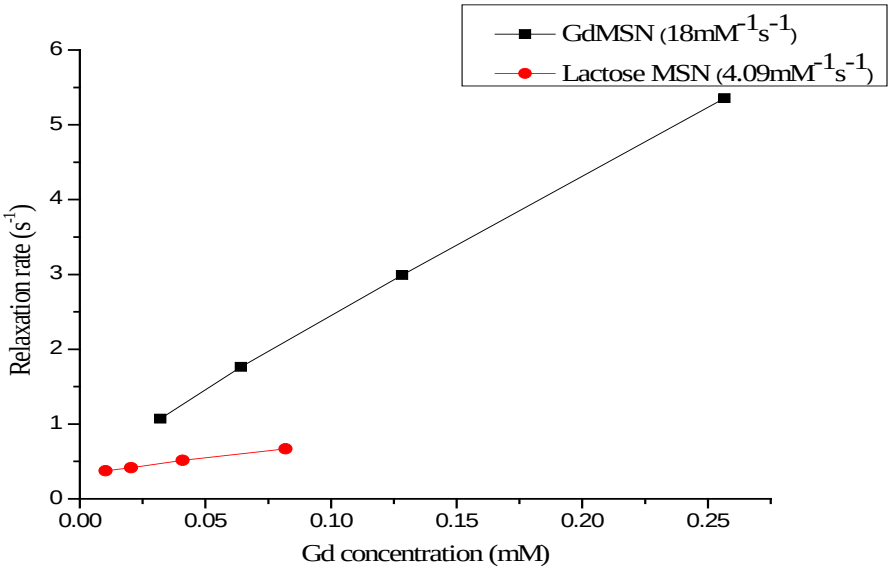

Figure 4.5: Graph to determine decrease in relaxivity (relaxivity values r_1 are shown in bracket)

The 75% decrease in relaxivity is an indication of the presence of the lactose cap that blocks access of water molecules to the internally bound Gd contrast agent. The observance of 25%

relaxivity would be attributed to the Gd-doping on the external surface of the MSN that is easily accessible by water molecules. This may also be due to lack of 100% coverage by lactose molecules.

4.7. Enzymatic Removal of Lactose Cap:

Lactose is hydrolysed in the presence of the enzyme beta-galactosidase that is produced intracellularly in *E.coli* cells as a part of the lac operon (Introduction chapter) [91]. Thus the commercially available beta-galactosidase was employed to study the release of payload on hydrolysis of lactose *in vitro*. The enzymatic assay included phosphate buffer, magnesium chloride and beta-mercaptoethanol. This assay absorbs between 200-250 nm on the UV and hence it is difficult to follow AITC release (since AITC absorbs at 245 nm). Thus, rhodamine 6G loaded lactose MSNs were used in the study with the enzymatic assay to follow the release of rhodamine 6G at 529 nm on the UV Spectrophotometer.

However, minimal release (1µg of rhodamine 6G from 60mg of particle sample) was observed in the presence of the enzyme beta-galactosidase in the enzymatic assay over 48 hours of stirring for each differing conditions (Experimental chapter).Repetition of assay was carried out at least 4-5 times along with varying the MSN and enzyme concentrations, all of which did not give release of rhodamine 6G. This is attributed to the following reasons:

- The enzyme is unable to approach the lactose due to restricted access
- Enzyme may be getting immobilised on the nanoparticle
- The enzyme may be inactive

To test the activity of the enzyme, ortho-nitrophenylgalatoside (ONPG) was employed as the substrate. ONPG containing a galactose and an o-nitrophenol moiety is hydrolysed by beta-galactosidase [93]. The solution thus turns yellow due to the presence of o-nitrophenol, followed spectroscopically at 410 nm. As expected, the UV absorption at 410 nm was observed, proving that the enzyme was active in the assay.

Therefore, the lactose capping was seen to be an appropriate stopper for the oil and water molecules. However, the enzymatic release from rhodamine 6G loaded lactose MSNs was unsuccessful which may be due to the immobilisation of the enzyme on the nanoparticle or the restricted access of the enzyme to its substrate. There have been published reports[60, 66, 67] demonstrating enzymatic release of encapsulated drug or dye, however these have been with different enzyme-cap systems and in some cases the conditions of enzymatic hydrolysis were unclear.

It is hoped that the ingestion of nanoparticles inside the bacterial cells and enzymatic hydrolysis *in situ* would be more effective. Also, it is expected that the toxic dosage required from nanoparticles would be much lower than that observed for pure oil. Thus, incubation of bacterial cells with oil-loaded lactose capped MSNs was carried out as discussed below.

4.8. Bacterial Incubation to Study Antibacterial Activity of Loaded Nanoparticles:

To establish the antibacterial activity of the AITC loaded lactose capped MSNs, incubation with *E.coli* cells was performed. Even though the *ex situ* enzymatic release study was

unsuccessful, cell viability studies were carried out in order to study antibacterial effects of the loaded nanoparticles.

From the oil-release studies reported earlier, 12 mg/ml of AITC loaded lactose MSNs would be required to achieve the toxic dosage of 625 mg/L. However, it is expected that the actual concentration for antibacterial toxicity would be much less than 12 mg/ml of nanoparticle suspension. This is expected since encapsulation of the oil within the mesopores reduces its loss due to volatility and MSNs are readily miscible in the phosphate buffer bacterial suspension. It was hoped that MSNs would then present a much more effective means of oil delivery. Hence, incubation studies were performed with 1 mg/ml and 5 mg/ml of AITC-lactose MSN solutions.

Comparing the data with unloaded lactose MSNs cell toxicity studies reported earlier, it is noted that 1 mg/ml AITC-lactose MSNs reduce the cell viability by 26% and are cytotoxic to the bacteria at these concentrations (Table 4.3). These nanoparticles have delivered an AITC dosage of nearly 0.05 mg/ml compared to the 0.625 mg/mL dosage required from oil toxicity studies- a 12.5 fold decrease in dosage. Thus, the lactose coated nanoparticle system doped with AITC has a higher efficacy against *E.coli* compared to the pure oil. The MSN system prevents loss of AITC on encapsulation and increases antibacterial efficacy due to its hydrophilicity. The lactose-capped release mechanism is successful in *in vitro* studies. Hence, a targeted and efficient delivery system has been achieved to deliver the antibacterial oils to *E.coli* cells.

Table 4.3: Cell viability for *E.coli* cells incubated with 1 mg/ml and 5 mg/ml AITC-Lactose MSNs in phosphate buffer solutions:

Cells	Viability (live bacteria)
Control with just cells	78.8 ± 5 %
1 mg/ml empty lactose MSNs	81.3 ± 5 %
5 mg/ml empty lactose MSNs	63.3 ± 6 %
1 mg/ml AITC-lactose MSN	55.1 ± 4 %
5 mg/ml AITC-lactose MSN	53.1 ± 4 %

Due to the successful uptake, release and antibacterial potency, the applications of these oil-loaded lactose MSNs towards bacterial biofilms may be further investigated. Preliminary work with biofilms is discussed.

4.9. Bacterial Biofilm Confocal Study:

A secondary application of treating a bacterial biofilm with AITC doped lactose MSN is being investigated. A bacterial biofilm consists of aggregates of bacteria in which cells adhere to each other and/or to a surface. These are embedded within a self-produced matrix of extracellular polymeric substance (EPS) that is a polymeric conglomeration generally composed of extracellular DNA, proteins and polysaccharides. These biofilms are more robust than bacterial cells. Preliminary work with bacterial biofilm includes their incubation with AITC and unloaded fluorescent MSNs (1 mg/ml).

Spectral confocal analysis was performed on the following biofilms (Experimental chapter):

- (Control) Biofilm without oil or fluorescent MSN
- Biofilm treated with 625 mg/L of AITC

- Biofilm treated with fluorescent MSN (1mg/mL)

For confocal imaging, the cells were stained with two dyes- green syto 9 (ex: 488nm; em: 500nm) that dyes both live and dead cells and red propidium iodide (ex: 488nm; em: 635nm) which dyes only the dead cells. The Fluorescent MSNs were dyed with red rhodamine (ex: 550nm; em: 610nm).

Confocal imaging shows the effect of treatment with the oils (Figure 4.7, right) and nanoparticles (Figure 4.8) with the control (Figure 4.7, left). In figure 4.7(left), the presence of only green colour is indicative of live cells in the control. After treatment with AITC, cell death is indicated by the yellow overlap observed (Figure 4.7, right). The non-toxicity of the nanoparticles is shown in figure 4.8. The left-hand image is gathered after the excitation and emission of the green and red dyes only. The green emission indicates only live cells. The right-hand image (Figure 4.8) is resolved by exciting the green dye and the red f-MSNs. The presence of yellow overlap indicates uptake of f-MSNs by the biofilm.

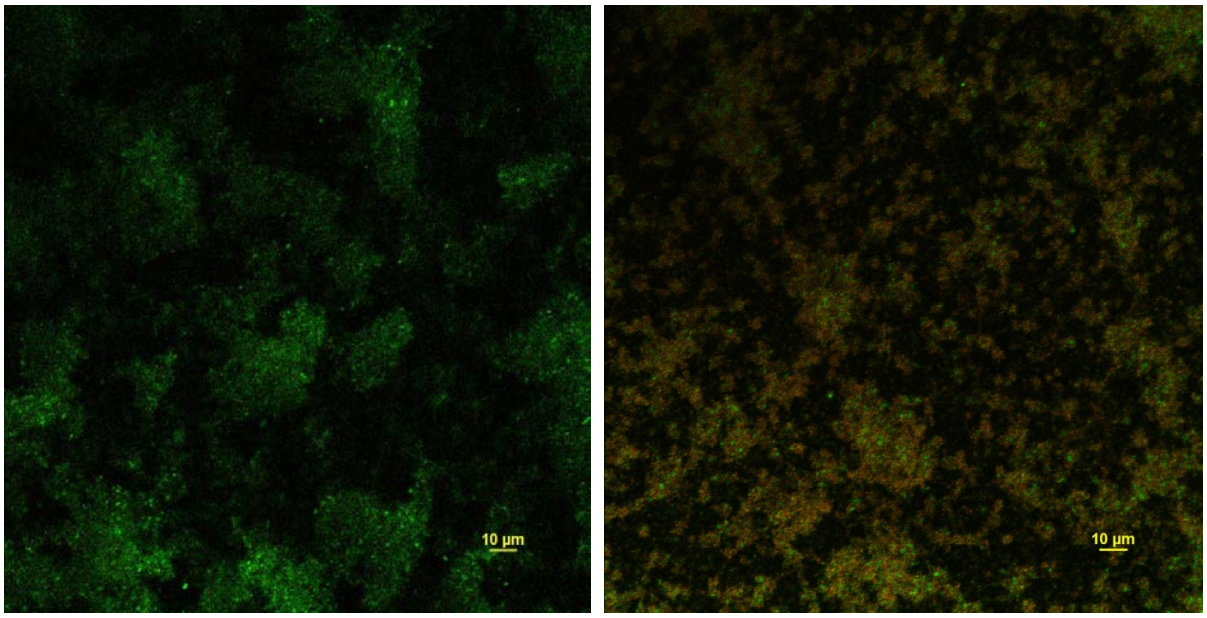

Figure 4.7: Bacterial biofilm: (left) Control (right) Biofilm doped with AITC: The confocal images show control biofilm (left) to be totally green due to absence of any dead cells (indicated by red dye). Imaging of a biofilm doped with 625 mg/L of AITC (right) indicates the presence of dead cells due to the yellow overlap of all cells (green) with dead cells (red).

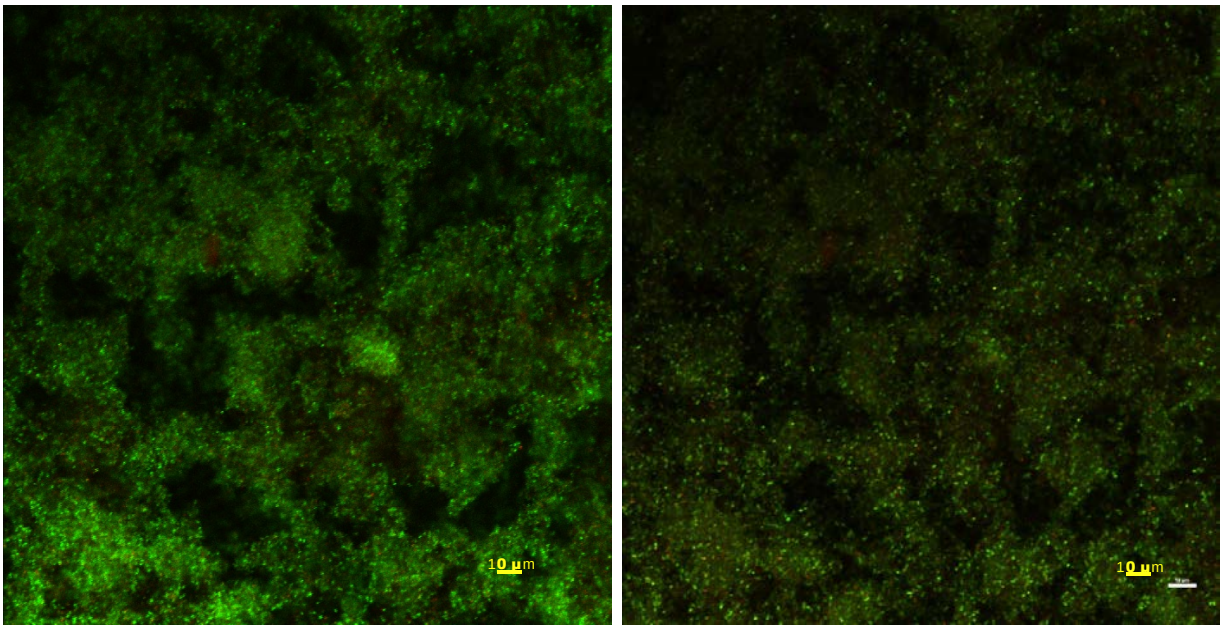

Figure 4.8: Biofilm doped with f-MSN to observe native particle non-toxicity: (left) Imaging of f-MSN treated biofilm excited at 488 nm (em: 500 nm) for green and 488nm (em: 635 nm) for red wavelengths confirms an absence of cell death (after 24 hours in 1 mg/ml dosage) – see left. The particles themselves are separately resolved by excitation at 550 nm (em: 610 nm) (right).
The left-hand image being green indicates presence of live cells only and hence confirms particle nontoxicity to bacteria. In the right-hand image, the presence of yellow overlap indicates the uptake of f-MSNs by the biofilm.

These investigations confirm that a dosage of 625 mg/L of AITC was cytotoxic to the biofilm (Figure 4.7). MSNs have also been shown as non-toxic towards bacterial biofilm, indicating that they can be suitably used as delivery agents for the oils. Further work involving incubation of AITC loaded lactose MSNs with bacterial biofilms is proposed.

4.10. Conclusions:

Mesoporous silica nanoparticles have been demonstrated as antibacterial oil delivery agents. The loading and release characteristics of these oils inside the mesopores of MSNs has been optimised. The role of lactose as a cap was demonstrated *via* oil and water retention in the mesopores. The experiments to observe release of the payload *via* enzymatic hydrolysis of lactose *ex situ* were however less successful. Thus, to ascertain antibacterial efficacy and higher reactivity to enzymatic hydrolysis on bacterial ingestion, AITC loaded lactose MSNs were incubated with *E.coli* cells. Preliminary work has shown them to be toxic in doses significantly lower than the pure oil. The oil-encapsulated MSNs are readily miscible in buffer solutions for *E.coli* cell work that rendered hydrophilicity and decreased loss due to volatility. The particles were determined to be cytotoxic to bacterial cells in concentrations of 1 mg/ml while delivering a dosage that was 12.5 times lower than the MIC dosage of the pure oil. Thus, successful and highly efficient delivery of antibacterial oils to *E.coli* cells was achieved. Very little has been reported on the use of nanoparticles for delivery of these oils. A recent study[105] reported the use of unfunctionalised uncapped mesoporous silica nanoparticles with pore diameters of 6.8-7.8 nm to deliver AITC vapours to study antibacterial toxicity against different bacterial species including *E.coli*, *Stapphylococcus aureus* and *Salmonella*

typhi. As expected, there was a delay in cell killing ranging from 48-72 hours due to the slower vapour action. In comparison, our oil loaded and lactose capped MSNs were successful in oil encapsulation for targeted delivery and reduced cell viability within 18 hours of incubation.

Preliminary studies with bacterial biofilms showed cytotoxicity of the oils against these biofilms. Their incubation and imaging with 1 mg/ml f-MSNs showed cellular internalisation and non-toxicity in biofilms. Thus, nanoparticle systems may be further studied as antibacterial agents against these bacterial biofilms.

5. CONCLUSIONS AND FUTURE WORK

In this work, native and functionalised mesoporous silica nanoparticles were prepared and investigated for their use as antibacterial delivery vehicles. These antibacterial loaded MSN composites are particularly useful and contribute significantly to the developing field of nanomedicine. MSNs have been successfully synthesised *via* silica condensation and hydrolysis using CTAB as a removable template. They have been reliably functionalised with amino, carboxyl, PEG and lactose groups and characterised using DLS, zeta potential, TEM, TGA, FTIR and nitrogen adsorption-desorption. The MSNs were found to be spherical, homogeneous and colloidally stable in suspension with diameters ranging from 55-75 nm and pore size of 3.6 nm (Table 3.1, 3.2). On amine modification and facilitated subsequent lactose coupling, the spherical shape, homogeneity and colloidal stability of the resulting nanoparticles were retained. Successful surface functionalisation of groups including APTES and lactose was confirmed using zeta potential, FTIR and TGA.

An investigation of cell uptake characteristics of fluorescent MSNs and PEG-functionalised f-MSNs was carried out by incubation with HeLa cells. Confocal analysis of the f-MSNs (0.1 mg/ml) with HeLa cells confirmed internalisation and uptake by endocytosis within the lysosomes. This took place within 3 hours of incubation. However, PEG-MSNs were internalised only after 30 hours of incubation indicating that the PEG chain contributed to longer circulation and delayed cellular internalisation.

Loading of AITC and cinnamaldehyde within the mesopores of the MSNs was performed to determine their delivery dosage and release kinetics from MSNs. The release kinetics showed

a rapid release of the loaded oil in the absence of a stopper within the first 5 hours and hence the need to cap. Lactose for chosen as a suitable cap due to its biocompatibility and prospective bio-triggered hydrolysis in bacterial cells such as *E.coli*.

In order to explore this sugar's capping and release mechanism, lactose was coupled onto MSNs via nucleophilic substitution. The reaction was catalysed by an acid, pyridinium para-toluene sulphonate (PPTS) since prior attempts in absence of any catalysts failed to indicate successful capping, giving inconsistent zeta potential results on surface charge modification.

In this work, an optimised protocol for lactose coupling incorporating PPTS was formulated, which appeared to both shut off water access to mesopore interior and cap entrapped organic oil or dye. Oil loading inside the mesopores of the capped MSNs was determined to be 5% by weight using TGA, also supported by uptake-release studies from uncapped MSNs.

Experiments to study the release of the payload *via* enzymatic hydrolysis of lactose *ex situ* were unsuccessful. Since the enzyme was deemed to be active, this was attributed to the possibilities of enzyme immobilisation and the restricted geometric access of enzyme to its substrate. Thereafter, antibacterial activity on bacterial ingestion was achieved by incubation of the oil loaded lactose MSNs with *E.coli* cells. The particles were shown to be cytotoxic to bacterial cells in concentrations of 1 mg/ml, while delivering a dosage that was 12.5 times lower than the MIC dosage of the pure oil (Table 4.3). This is a significant decrease in toxic dosage required for cell death. This result indicates the enormous potential of MSNs as drug

delivery agents- not only allowing delivery to a targeted system, but also potentially and dramatically decreasing the amount of drug required.

Overall, our system of loading mesoporous silica nanoparticles, with antibacterial oils and subsequent capping with lactose was an efficient and colloidally stable delivery system that achieved *E.coli* cell killing *in vitro* at markedly lower doses than the pure oil.

Future work in this direction would involve achieving higher loading of oil in particles by investigating hollow MSNs and polymeric nanoparticles. The investigation of the antibacterial effects with other oil loaded lactose capped MSNs would also be explored. Once the antibacterial toxicity of these MSNs with bacterial cells has been optimised, additional studies with bacterial biofilms would be undertaken.

Additionally, the challenges of investigating the release *via* enzymatic hydrolysis *ex situ* would be probed. In this view, chemical hydrolysis treatments would be analysed that bring about lactose hydrolysis without destroying the nanoparticles' morphology.

Further applications of the lactose capped MSN system would be in direct targeting to *E.coli* cells in a suspension of different bacterial species. This would mainly exploit the targeting ability of lactose towards only *E.coli* cells. Work in this direction would involve initial studies on the interactions of different bacteria with one another and with lactose.

It is believed that these drug delivery composites have excellent potential for bacterial cell targeting. They could be envisaged as materials for water treatment as well as showing promise in antimicrobial surface coating technologies, which will be developed in future.

APPENDICES

6.1. FTIR Spectra:

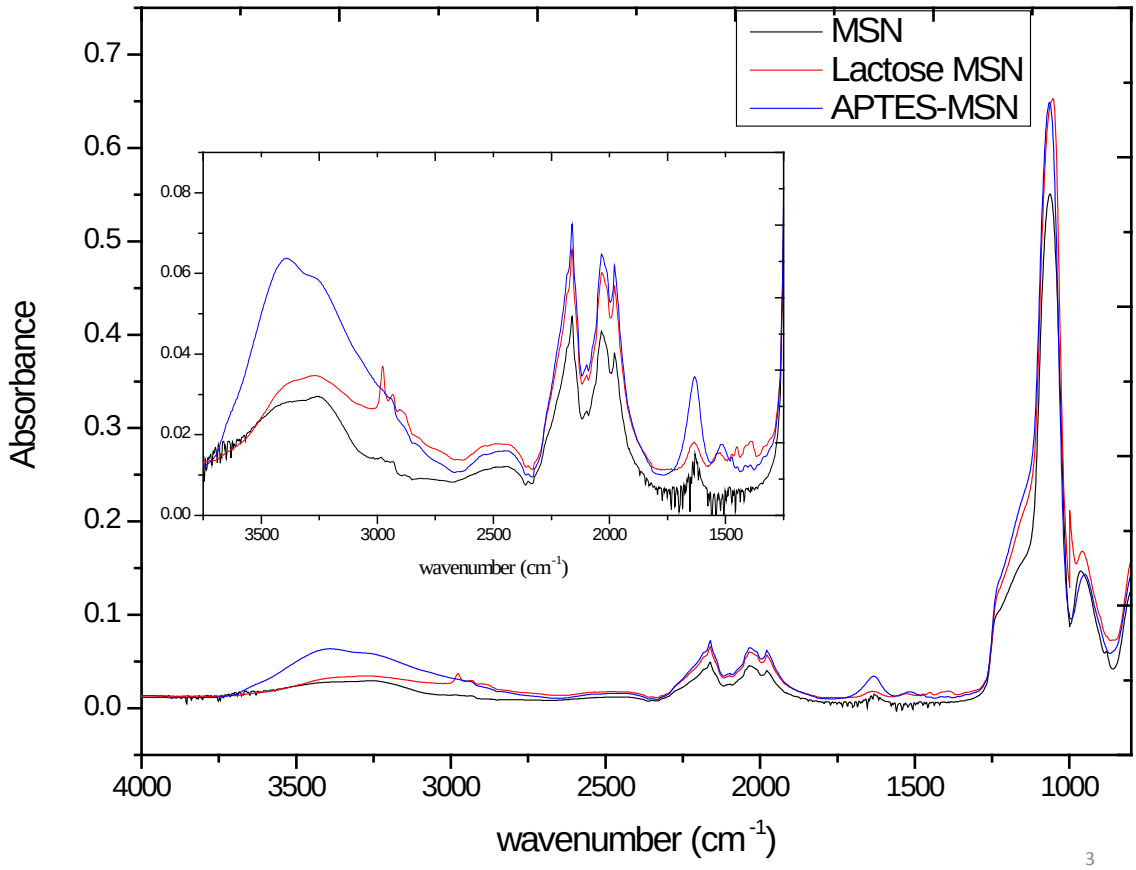

Figure 6.1: FTIR spectra for unfunctionalised (black), aminated (blue) and lactose MSNs (red). Inset shows close of 1250-4000 cm^{-1}.

6.2. E.coli cell- lactose Fluorescent MSN Internalisation:

The *E.coli* cells were grown as stated in the Experimental chapter and incubated for 20 hours with lactose-capped fluorescent MSNs. The cells were then transferred to a 2 ml petridish, stained with syto 9 (green dye, ex: 488 nm; em: 500 nm), washed with PBS and imaged on the confocal laser scanning microscopy.

The image shows yellow emission from a single cell arising from both the syto 9 stain and the presence of internalised f-MSN nanoparticle.

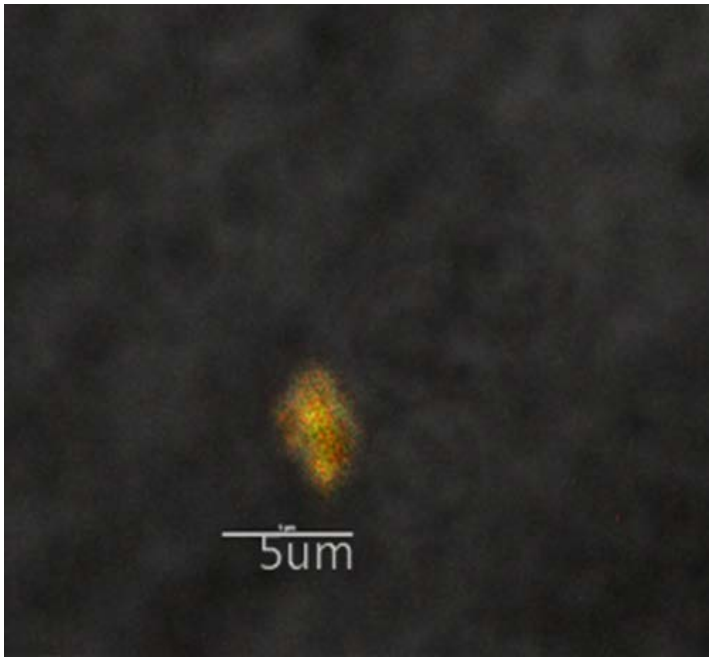

Figure 6.2: Confocal image of the yellow overlap of a single *E.coli* cell (dyed with green) with lactose coated f-MSN (red) showing its internalisation.

6.3. UV-Visible Spectra:

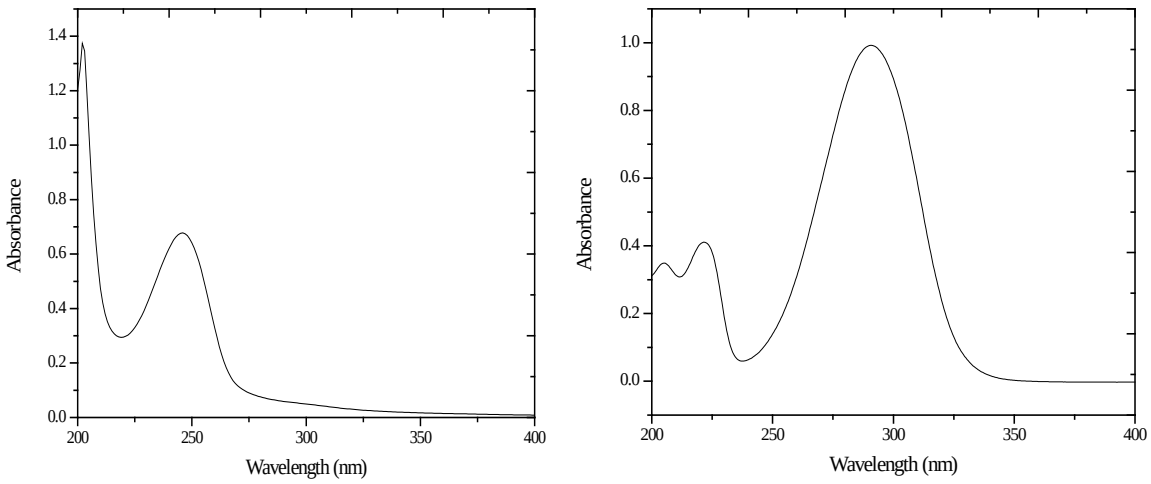

Figure 6.3: UV-Visible spectra for the essential oils- allyl isothiocyanate (left) and cinnamaldehyde (right) showing peaks at 245 nm and 291 nm respectively.

REFERENCES

1. J. Gao and B. Xu, *Nano Today*, 2009, **4**, 37-51.
2. A. Bernardos, L. Mondragon, E. Aznar, M. D. Marcos, R. Martinez-Manez, F. Sancenon, J. Soto, J. M. Barat, E. Perez-Paya, C. Guillem and P. Amoros, *Acs Nano*, 2010, **4**, 6353-6368.
3. J. F. Chen, H. M. Ding, J. X. Wang and L. Shao, *Biomaterials*, 2004, **25**, 723-727.
4. K. K. Coti, M. E. Belowich, M. Liong, M. W. Ambrogio, Y. A. Lau, H. A. Khatib, J. I. Zink, N. M. Khashab and J. F. Stoddart, *Nanoscale*, 2009, **1**, 16-39.
5. P. DeMuth, M. Hurley, C. W. Wu, S. Galanie, M. R. Zachariah and P. DeShong, *Microporous and Mesoporous Materials*, 2011, **141**, 128-134.
6. Q. J. He, J. L. Shi, F. Chen, M. Zhu and L. X. Zhang, *Biomaterials*, 2010, **31**, 3335-3346.
7. J. Kim, H. S. Kim, N. Lee, T. Kim, H. Kim, T. Yu, I. C. Song, W. K. Moon and T. Hyeon, *Angewandte Chemie-International Edition*, 2008, **47**, 8438-8441.
8. C. Y. Lai, B. G. Trewyn, D. M. Jeftinija, K. Jeftinija, S. Xu, S. Jeftinija and V. S. Y. Lin, *Journal of the American Chemical Society*, 2003, **125**, 4451-4459.
9. J. E. Lee, N. Lee, H. Kim, J. Kim, S. H. Choi, J. H. Kim, T. Kim, I. C. Song, S. P. Park, W. K. Moon and T. Hyeon, *Journal of the American Chemical Society*, 2010, **132**, 552-557.
10. M. Liong, J. Lu, M. Kovochich, T. Xia, S. G. Ruehm, A. E. Nel, F. Tamanoi and J. I. Zink, *Acs Nano*, 2008, **2**, 889-896.
11. M. Liong, S. Angelos, E. Choi, K. Patel, J. F. Stoddart and J. I. Zink, *Journal of Materials Chemistry*, 2009, **19**, 6251-6257.

12. H. A. Meng, M. Xue, T. A. Xia, Y. L. Zhao, F. Tamanoi, J. F. Stoddart, J. I. Zink and A. E. Nel, *Journal of the American Chemical Society*, 2010, **132**, 12690-12697.

13. L. Pasqua, S. Cundari, C. Ceresa and G. Cavaletti, *Current Medicinal Chemistry*, 2009, **16**, 3054-3063.

14. J. M. Rosenholm, C. Sahlgren and M. Linden, *Nanoscale*, 2010, **2**, 1870-1883.

15. Slowing, II, B. G. Trewyn, S. Giri and V. S. Y. Lin, *Advanced Functional Materials*, 2007, **17**, 1225-1236.

16. Slowing, II, J. L. Vivero-Escoto, C. W. Wu and V. S. Y. Lin, *Advanced Drug Delivery Reviews*, 2008, **60**, 1278-1288.

17. Q. L. Tang, Y. Xu, D. Wu and Y. H. Sun, *Journal of Solid State Chemistry*, 2006, **179**, 1513-1520.

18. M. Vallet-Regi, A. Ramila, R. P. del Real and J. Perez-Pariente, *Chemistry of Materials*, 2001, **13**, 308-311.

19. M. Van Speybroeck, V. Barillaro, T. Do Thi, R. Mellaerts, J. Martens, J. Van Humbeeck, J. Vermant, P. Annaert, G. Van Den Mooter and P. Augustijns, *Journal of Pharmaceutical Sciences*, 2009, **98**, 2648-2658.

20. L. S. Wang, L. C. Wu, S. Y. Lu, L. L. Chang, I. T. Teng, C. M. Yang and J. A. A. Ho, *Acs Nano*, 2010, **4**, 4371-4379.

21. W. Stober, A. Fink and E. Bohn, *Journal of Colloid and Interface Science*, 1968, **26**, 62-69.

22. F. Caruso, R. A. Caruso and H. Mohwald, *Science*, 1998, **282**, 1111-1114.

23. G.-L. Davies, A. Barry and Y. K. Gun'ko, *Chemical Physics Letters*, 2009, **468**, 239-244.

24. A. Vanblaaderen, J. Vangeest and A. Vrij, *Journal of Colloid and Interface Science*, 1992, **154**, 481-501.

25. A. Vanblaaderen and A. Vrij, *Langmuir*, 1992, **8**, 2921-2931.

26. W. Stober, A. Fink and E. Bohn, *Journal of Colloid and Interface Science*, 1968, **26**, 62-&.

27. A. J. Di Pasqua, K. K. Sharma, Y. L. Shi, B. B. Toms, W. Ouellette, J. C. Dabrowiak and T. Asefa, *Journal of Inorganic Biochemistry*, 2008, **102**, 1416-1423.

28. Q. J. He, Z. W. Zhang, Y. Gao, J. L. Shi and Y. P. Li, *Small*, 2009, **5**, 2722-2729.

29. J. M. Hillegass, A. Shukla, S. A. Lathrop, M. B. MacPherson, N. K. Fukagawa and B. T. Mossman, *Wiley Interdisciplinary Reviews-Nanomedicine and Nanobiotechnology*, 2010, **2**, 219-231.

30. M. Fisichella, H. Dabboue, S. Bhattacharyya, G. Lelong, M. L. Saboungi, F. Warmont, P. Midoux, C. Pichon, M. Guerin, T. Hevor and J. P. Salvetat, *Journal of Nanoscience and Nanotechnology*, 2010, **10**, 2314-2324.

31. L. C. J. Thomassen, A. Aerts, V. Rabolli, D. Lison, L. Gonzalez, M. Kirsch-Volders, D. Napierska, P. H. Hoet, C. E. A. Kirschhock and J. A. Martens, *Langmuir*, 2010, **26**, 328-335.

32. Y. S. Lin and C. L. Haynes, *Journal of the American Chemical Society*, 2010, **132**, 4834-4842.

33. Y. L. Zhao, Z. X. Li, S. Kabehie, Y. Y. Botros, J. F. Stoddart and J. I. Zink, *Journal of the American Chemical Society*, 2010, **132**, 13016-13025.

34. M. J. K. Thomas, I. Slipper, A. Walunj, A. Jain, M. E. Favretto, P. Kallinteri and D. Douroumis, *International Journal of Pharmaceutics*, 2010, **387**, 272-277.

35. Y. Yang, W. X. Song, A. H. Wang, P. L. Zhu, J. B. Fei and J. B. Li, *Physical Chemistry Chemical Physics*, 2010, **12**, 4418-4422.

36. Y. N. Zhao, B. G. Trewyn, Slowing, II and V. S. Y. Lin, *Journal of the American Chemical Society*, 2009, **131**, 8398-+.

37. N. Gartmann and D. Bruehwiler, *Angewandte Chemie-International Edition*, 2009, **48**, 6354-6356.

38. J. Xie, S. Lee and X. Y. Chen, *Advanced Drug Delivery Reviews*, 2010, **62**, 1064-1079.

39. S. Calmettes, B. Albela, O. Hamelin, S. Menage, F. Miomandre and L. Bonneviot, *New Journal of Chemistry*, 2008, **32**, 727-737.

40. K. McEleney, D. P. Allen, A. E. Holliday and C. M. Crudden, *Organic Letters*, 2006, **8**, 2663-2666.

41. D. J. Mihalcik and W. B. Lin, *Chemcatchem*, 2009, **1**, 406-413.

42. Q. S. Huo, J. L. Feng, F. Schuth and G. D. Stucky, *Chemistry of Materials*, 1997, **9**, 14-&.

43. K. K. Unger, D. Kumar, M. Grun, G. Buchel, S. Ludtke, T. Adam, K. Schumacher and S. Renker, *Journal of Chromatography A*, 2000, **892**, 47-55.

44. N. Andersson, P. C. A. Alberius, J. S. Pedersen and L. Bergstrom, *Microporous and Mesoporous Materials*, 2004, **72**, 175-183.

45. T. D. Nguyen, K. C. F. Leung, M. Liong, C. D. Pentecost, J. F. Stoddart and J. I. Zink, *Organic Letters*, 2006, **8**, 3363-3366.

46. Y. L. Choi, J. Jaworski, M. L. Seo, S. J. Lee and J. H. Jung, *Journal of Materials Chemistry*, 2011, **21**, 7882-7885.

47. K. Moller, J. Kobler and T. Bein, *Advanced Functional Materials*, 2007, **17**, 605-612.

48. J. Kobler, K. Moller and T. Bein, *Acs Nano*, 2008, **2**, 791-799.

49. K. Moller, J. Kobler and T. Bein, *Journal of Materials Chemistry*, 2007, **17**, 624-631.

50. A. B. D. Nandiyanto, S. G. Kim, F. Iskandar and K. Okuyama, *Microporous and Mesoporous Materials*, 2009, **120**, 447-453.

51. J. S. Beck, J. C. Vartuli, W. J. Roth, M. E. Leonowicz, C. T. Kresge, K. D. Schmitt, C. T. W. Chu, D. H. Olson, E. W. Sheppard, S. B. McCullen, J. B. Higgins and J. L. Schlenker, *Journal of the American Chemical Society*, 1992, **114**, 10834-10843.

52. S. Huh, J. W. Wiench, J. C. Yoo, M. Pruski and V. S. Y. Lin, *Chemistry of Materials*, 2003, **15**, 4247-4256.

53. T. Suteewong, H. Sai, J. Lee, M. Bradbury, T. Hyeon, S. M. Gruner and U. Wiesner, *Journal of Materials Chemistry*, 2010, **20**, 7807-7814.

54. A. B. Fuertes, P. Valle-Vigon and M. Sevilla, *Journal of Colloid and Interface Science*, 2010, **349**, 173-180.

55. Y. Z. Zhang, Z. Z. Zhi, T. Y. Jiang, J. H. Zhang, Z. Y. Wang and S. L. Wang, *Journal of Controlled Release*, 2010, **145**, 257-263.

56. J. M. Rosenholm and M. Linden, *Chemistry of Materials*, 2007, **19**, 5023-5034.

57. J. M. Rosenholm, A. Duchanoy and M. Linden, *Chemistry of Materials*, 2008, **20**, 1126-1133.

58. J. Kecht, A. Schlossbauer and T. Bein, *Chemistry of Materials*, 2008, **20**, 7207-7214.

59. B. G. Trewyn, Slowing, II, S. Giri, H. T. Chen and V. S. Y. Lin, *Accounts of Chemical Research*, 2007, **40**, 846-853.

60. K. Patel, S. Angelos, W. R. Dichtel, A. Coskun, Y. W. Yang, J. I. Zink and J. F. Stoddart, *Journal of the American Chemical Society*, 2008, **130**, 2382-2383.

61. C. Park, K. Lee and C. Kim, *Angewandte Chemie-International Edition*, 2009, **48**, 1275-1278.

62. O. Hocine, M. Gary-Bobo, D. Brevet, M. Maynadier, S. Fontanel, L. Raehm, S. Richeter, B. Loock, P. Couleaud, C. Frochot, C. Charnay, G. Derrien, M. Smaihi, A. Sahmoune, A. Morere, P. Maillard, M. Garcia and J.-O. Durand, *International Journal of Pharmaceutics*, 2010, **402**, 221-230.

63. N. K. Mal, M. Fujiwara and Y. Tanaka, *Nature*, 2003, **421**, 350-353.

64. D. P. Ferris, Y. L. Zhao, N. M. Khashab, H. A. Khatib, J. F. Stoddart and J. I. Zink, *Journal of the American Chemical Society*, 2009, **131**, 1686-+.

65. S. Saha, K. C. F. Leung, T. D. Nguyen, J. F. Stoddart and J. I. Zink, *Advanced Functional Materials*, 2007, **17**, 685-693.

66. A. Bernardos, E. Aznar, M. D. Marcos, R. Martinez-Manez, F. Sancenon, J. Soto, J. M. Barat and P. Amoros, *Angewandte Chemie-International Edition*, 2009, **48**, 5884-5887.

67. C. Park, H. Kim, S. Kim and C. Kim, *Journal of the American Chemical Society*, 2009, **131**, 16614-+.

68. E. Climent, R. Martinez-Manez, F. Sancenon, M. D. Marcos, J. Soto, A. Maquieira and P. Amoros, *Angewandte Chemie-International Edition*, 2010, **49**, 7281-7283.

69. L. Du, S. Liao, H. A. Khatib, J. F. Stoddart and J. I. Zink, *Journal of the American Chemical Society*, 2009, **131**, 15136-15142.

70. Q. A. Gao, Y. Xu, D. Wu, W. L. Shen and F. Deng, *Langmuir*, 2010, **26**, 17133-17138.

71. H. Kim, S. Kim, C. Park, H. Lee, H. J. Park and C. Kim, *Advanced Materials*, 2010, **22**, 4280-+.

72. I. Sondi and B. Salopek-Sondi, *Journal of Colloid and Interface Science*, 2004, **275**, 177-182.

73. A. Panacek, L. Kvitek, R. Prucek, M. Kolar, R. Vecerova, N. Pizurova, V. K. Sharma, T. j. Nevecna and R. Zboril, *Journal of Physical Chemistry B*, 2006, **110**, 16248-16253.

74. J. R. Morones, J. L. Elechiguerra, A. Camacho, K. Holt, J. B. Kouri, J. T. Ramirez and M. J. Yacaman, *Nanotechnology*, 2005, **16**, 2346-2353.

75. C. Baker, A. Pradhan, L. Pakstis, D. J. Pochan and S. I. Shah, *Journal of Nanoscience and Nanotechnology*, 2005, **5**, 244-249.

76. J. A. Spadaro, T. J. Berger, S. D. Barranco, S. E. Chapin and R. O. Becker, *Antimicrobial Agents and Chemotherapy*, 1974, **6**, 637-642.

77. B. G. Trewyn, C. M. Whitman and V. S. Y. Lin, *Nano Letters*, 2004, **4**, 2139-2143.

78. E. M. Hetrick, J. H. Shin, N. A. Stasko, C. B. Johnson, D. A. Wespe, E. Holmuhamedov and M. H. Schoenfisch, *Acs Nano*, 2008, **2**, 235-246.

79. S. Burt, *International Journal of Food Microbiology*, 2004, **94**, 223-253.

80. K. Palaniappan and R. A. Holley, *International Journal of Food Microbiology*, 2010, **140**, 164-168.

81. S. Prabuseenivasan, M. Jayakumar and S. Ignacimuthu, *BMC Complement Altern Med*, 2006, **6**, 39.

82. M. Turgis, J. Han, S. Caillet and M. Lacroix, *Food Control*, 2009, **20**, 1073-1079.

83. I. M. Helander, H. L. Alakomi, K. Latva-Kala, T. Mattila-Sandholm, I. Pol, E. J. Smid, L. G. M. Gorris and A. von Wright, *Journal of Agricultural and Food Chemistry*, 1998, **46**, 3590-3595.

84. S. Tunc, E. Chollet, P. Chalier, L. Preziosi-Belloy and N. Gontard, *International Journal of Food Microbiology*, 2007, **113**, 263-270.

85. Z. T. Jiang, Q. F. Zhang, H. L. Tian and R. Li, *Food Technology and Biotechnology*, 2006, **44**, 423-427.

86. T. Nuryastuti, H. C. van der Mei, H. J. Busscher, S. Iravati, A. T. Aman and B. P. Krom, *Applied and Environmental Microbiology*, 2009, **75**, 6850-6855.

87. H. J. D. Dorman and S. G. Deans, *Journal of Applied Microbiology*, 2000, **88**, 308-316.

88. N. Garg, S. Martini, D. W. Britt and M. K. Walsh, *Food Research International*, 2010, **43**, 1111-1115.

89. X. Auvray, C. Petipas, R. Anthore, I. Ricolattes and A. Lattes, *Langmuir*, 1995, **11**, 433-439.

90. J. G. Erickson, *Journal of the American Chemical Society*, 1955, **77**, 2839-2843.

91. D. H. Juers, T. D. Heightman, A. Vasella, J. D. McCarter, L. Mackenzie, S. G. Withers and B. W. Matthews, *Biochemistry*, 2001, **40**, 14781-14794.

92. K. Wallenfels, *The Enzymes*, Academic press, 1972.

93. G. R. Craven, E. Steers and C. B. Anfinsen, *Journal of Biological Chemistry*, 1965, **240**, 2468-&.

94. J. A. Hill and R. E. Huber, *Biochimica Et Biophysica Acta*, 1971, **250**, 530-&.

95. S. Shifrin, Grochows.Bj and S. W. Luborsky, *Nature*, 1970, **227**, 608-&.

96. M. Weyland, P. A. Midgley, R. Brydson, A. R. Lupini, S. N. Rashkeev, M. Varela, A. Y. Borisevich, M. P. Oxley, K. van Benthem, Y. Peng, N. de Jonge, G. M. Veith, S. T. Pantelides, M. F. Chisholm, S. J. Pennycook, R. E. Dunin–Borkowski, T. Kasama, R. J. Harrison, D. J. Smith, P. L. P.L. Gai, M. R. Castell, J. Hutchison and A. Angus Kirkland, *Nanocharacterisation*, Royal Society of Chemistry, 2008.

97. D. Pavia, G. M. Lampman, G. Kriz and J. Vyvyan, *Introduction to Spectroscopy*, fourth edition edn., Beokes/Cole Cengage Learning, 2009.

98. B. Stuart, John Wiley and Sons, Editon edn., 2004.

99. C. T. Chung, S. L. Niemela and R. H. Miller, *Proceedings of the National Academy of Sciences of the United States of America*, 1989, **86**, 2172-2175.

100. V. Cauda, A. Schlossbauer, J. Kecht, A. Zurner and T. Bein, *Journal of the American Chemical Society*, 2009, **131**, 11361-11370.

101. F. Thielbeer, K. Donaldson and M. Bradley, *Bioconjugate Chemistry*, 2011, **22**, 144-150.

102. G. Wang, A. N. Otuonye, E. A. Blair, K. Denton, Z. Tao and T. Asefa, *Journal of Solid State Chemistry*, 2009, **182**, 1649-1660.

103. H. Du, R. C. A. Fuh, J. Z. Li, L. A. Corkan and J. S. Lindsey, *Photochemistry and Photobiology*, 1998, **68**, 141-142.

104. F. Carniato, L. Tei, M. Cossi, L. Marchese and M. Botta, *Chemistry-a European Journal*, 2010, **16**, 10727-10734.

105. S.-Y. Park, M. Barton and P. Pendleton, *Food Control*, 2012, **23**, 478-484.